HIGH THROUGHPUT AUTOMATED SEEDLING PHENOTYPING SYSTEM

By

Ram Subramanian

A Dissertation submitted in partial fulfillment of the

requirements for the degree of

Doctor of Philosophy

(Mechanical Engineering)

at the

UNIVERSITY OF WISCONSIN – MADISON

2012

Date of final oral examination: 04/13/12

The dissertation is approved by the following members of the Final Oral Committee:

Nicola J. Ferrier, Professor, Mechanical Engineering

Edgar P Spalding, Professor, Botany

Dan Negrut, Associate Professor, Mechanical Engineering

Michael R Zinn, Assistant Professor, Mechanical Engineering

Li Zhang, Assistant Professor, Computer Science

Abstract

This thesis describes the design, development and analysis of a system to aid in automated phenotyping of seedlings in controlled environments. The task of phenotyping involves observing physical or behavioral changes (phenotype) in a plant as a consequence of an alteration to a particular gene (genetic mutation) in its genome. One method currently gaining a lot of interest for phenotype observation and analysis is the use of camera based acquisition and analysis. But with plant genomes containing upwards of 10^4 genes, comprehensive studies will require automated, high throughput methodologies.

To address this automation and throughput requirement without sacrificing spatial or temporal resolution, a robotic gantry system utilizing visual servoing and a sample-holding fixture were developed. A 1 m^2 sample fixture holds 36 Petri plates in which seedlings grow along the surface of agar gel perpendicular to the optical axis of two 2 CCD cameras with macro lenses, mounted on the end effector. One camera collects images at low magnification to aid in positioning and the other collects experimental data at higher magnification. Direct drive linear servo motors move the payload at a speed of 1 m/s with an accuracy of 1 μm, and a repeatability of 0.1 μm. A probabilistic image analysis algorithm are used to locate the root of seedlings in the Petri plate and a normalized gray scale variance measure was used to focus the camera on the root. The typical size of a root is about 45 to 200 μm wide and about 4 mm in length. The custom hardware and software together provide a robust seedling imaging platform capable of tracking growth of 72 roots (2 seedlings per Petri plate) in parallel at approximately 3 min intervals. The time series of images are then be subjected to phenotypic analysis for studies of gene function. The entire workflow is designed to have minimal human intervention.

Acknowledgments

I would like to thank all those on my committee Prof. Ferrier, Prof. Spalding, Prof. Zinn, Prof. Negrut and Prof. Zhang. I would especially like to thank my advisers Prof. Ferrier and Prof. Spalding for their support and guidance . A special thanks to Prabu Ravindran, Saigopal Nelaturi and Suman Mamidi for being a sounding board whenever I need them.

I am also thankful to my my wife - Nandini, brother - Raj and parents - the Subramanians, for their patience (especially my wife :-)) and support.

I would also like to thank Matt Boyd, Liz Henry, Kelsey Rudd, Logan Johnson, Nick Dimick, Lester Donic and Greg Johnson who provided timely help in the building of parts of the system. I owe thanks to the members of the Robotics and Intelligent Systems Lab and the Spalding Lab for their contributions towards the project and for sitting through all my practice talks.

I would finally like to thank, in advance, all those researchers who will someday make use of this system for their phenotyping research.

Contents

List of Figures

List of Tables

Chapter 1

Motivation

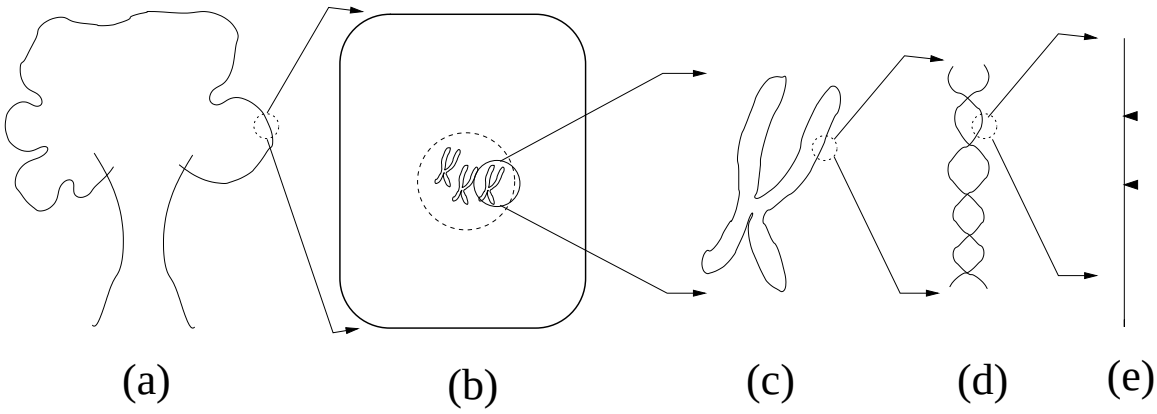

Figure 1.1. Genotypes and the genome. (a)Plant. (b)Cell. (c)Chromosome. (d)DNA. (e)Gene.

The genome of an organism is a collection of thousands of genes (approximately 10^4, in the case of plants). Genes are the functional regions or parts of a Deoxyribo Nucleic Acid (DNA) molecule. Each gene contains a chemical code or instruction to synthesize a protein and perform a specific function within the organism. The genes are arranged in the DNA molecules to give DNA its signature double helix structure (see figure 1.1). Within the nucleus of a cell these DNA molecules are coiled up into strands called chromosomes (a typical human genome has 23 pairs of chromosomes

while plants like *Arabidopsis thaliana* have 5).

The collective expression of these genes form an organism. A central topic of research in the field of plant biology is the study of processes by which the genome of a particular species produces an *observable biology*. The *observable biology* can range from physical parts (e.g. cellular structures), metabolic activity (e.g. production of certain proteins), to response to stimulus (root responding to the action of gravity, plant moving towards sunlight), i.e. physiology, morphology and behavior (the *phenome*) of the plant [22]. Each of these characteristics are the phenotypes of the plant. All of these phenotypes are controlled by genes or some subset of the genome, or a genotype (in other words the genotype *codes* the phenotype). The process of determining the phenotype for a genotype is generally termed as phenotyping. The most common methodology adopted for phenotype studies is to determine phenotype differences between a plant that has a modified genome and one that does not have any alterations to its genome. A plant with a modified genome (i.e. with a particular gene *knocked out*) is termed as a *mutant*. A plant with no alterations to its genome is called a *wild type*. Comparisons can be made between different parts of plants at various stages of development, be it seedling, sapling, seed or fully grown. The most commonly used model plant for phenotype studies is the *Arabidopsis thaliana.*

Highly sophisticated technologies drive the field of genomics (the study of gene sequences) but those for measuring the the phenotype, are typically crude by comparison, most commonly observations and measurements are carried out manually. Methods for measuring phenotype differences, however subtle, between mutant and wild type seedlings for large populations of a model plants, such as Arabidopsis thaliana, will provide critical clues about the biological function of the altered (mutant) gene. Any phenotype may manifest itself only transiently, hence any developed technique would

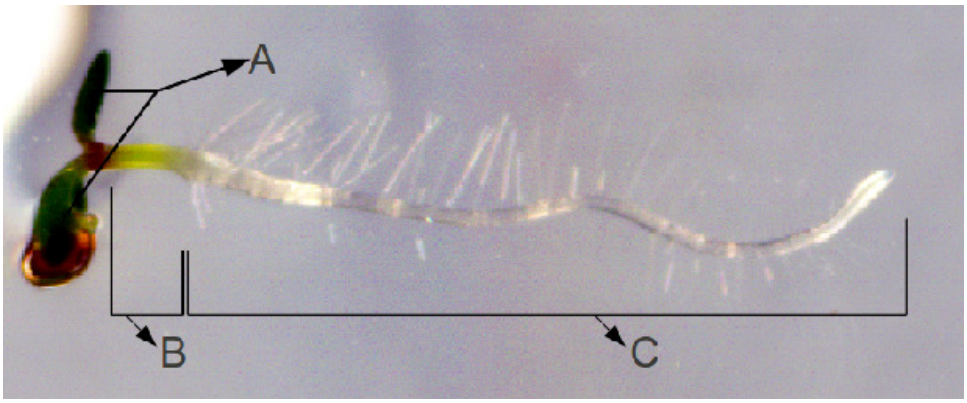

Figure 1.2. An example of a seedling imaged under infra red light. Parts of the seedling are labeled: (a) cotyledons (b) hypocotyl (c) root (d) seed coat.

need to have high spatio-temporal resolution. As the biological processes being monitored may be very subtle and sensitive to surrounding environmental conditions as they unfold, the techniques developed to monitor them must be non-invasive. Best progress in phenotyping will be achieved when data acquisition and analysis capacities and capabilities for both phenomics and genomics are matched. With most plants having on the order of 10^4 genes, and therefore a similar magnitude of mutants to be studied, phenotyping techniques would benefit from automation.

Machine vision techniques coupled with automation are well matched for these requirements. This has been recognized by several groups of researchers who developed machine vision approaches for plant growth monitoring, such as measuring the response to gravity for roots of the arabidopsis plant [2, 7, 8, 12, 13, 19, 23, 26, 31, 32, 33, 34]. These studies used a single camera to monitor each seedling and needed manual adjustment of the camera to ensure the seedling was correctly centered and focused in the acquired images. The use of multiple cameras can increase the throughput of observations (and the cost). Phenotype observations are typically taken with a time resolution on the order of minutes, over many hours. During the course of observation the cameras are in use only during the time period that an image is captured, the

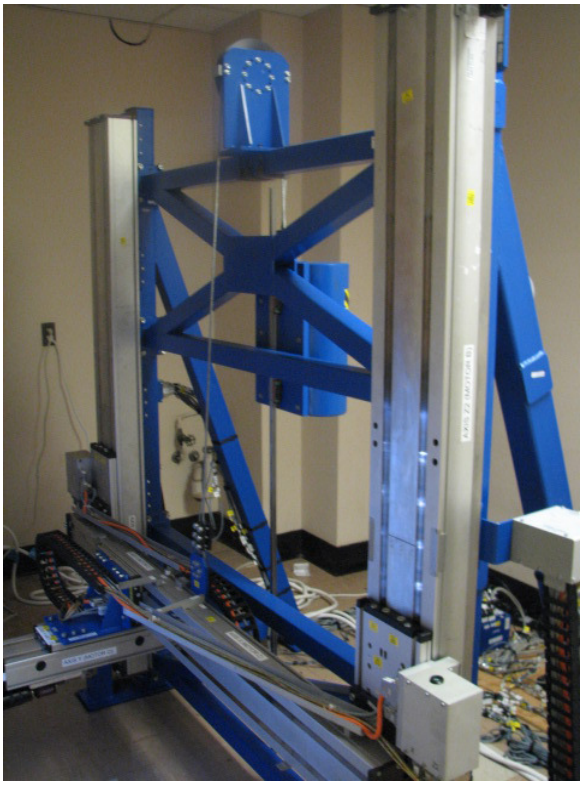

Figure 1.3. 3 Axis Gantry Robot

rest of the time the camera is idle. The time the camera is idle can be reduced by either moving the seedlings, one after the other, into the camera's field of view or by moving the camera in front of many seedlings one after the other. This reduces the idle time of the camera and increases the throughput. Here we choose to the perform the later using a robotic system to accurately position the camera to observe multiple seedlings.

There are emerging commercial efforts to automate data collection for plant phenotyping, e.g. [17], using a proprietary 3D scanner. This system moves potted plants to/from the scanner and uses x-rays to image the roots thus may not be suitable for some plant studies where plants are in the their seedling stage. Their 3D scanner can measure morphological features and has been used to observe leaves of the arabidop-

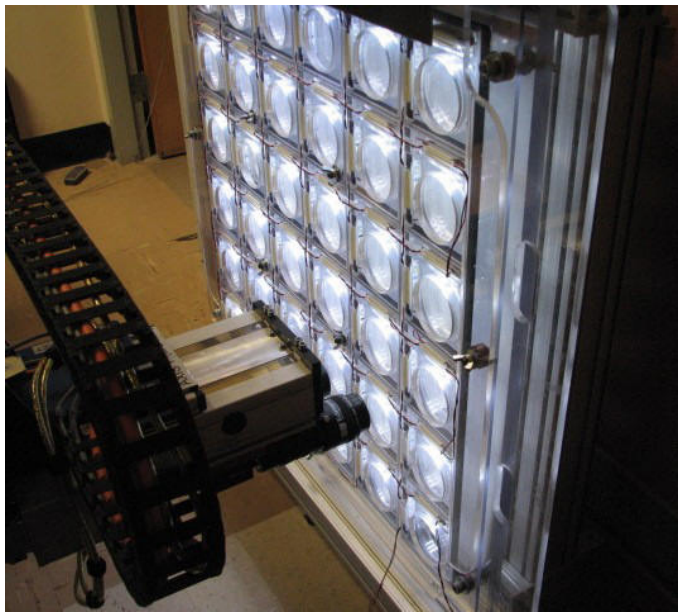

Figure 1.4. The robot system with the PDCU, grow lights and back lights.

sis. Movement of the germinating plant is undesirable (see e.g. [21]) and thus for our purposes, we sought an automated platform that would not disturb the developing plant.

The work presented here describes the development of an automated system that streamlines the task of planning, organizing, planting, imaging and analyzing seedling images and data. At the heart of the entire system is a gantry robot that uses visual feed back control (visual servoing) [5, 6] to localize and monitor the growth of numerous seedlings concurrently. The system consists of two primary parts, a Petri dish holder unit with controlled lighting to hold numerous plant seedlings and a visual servo controlled gantry robot. The robot identifies each seedling and tracks its growth over a specified time. Subsequently, the results of some data collected are presented. This system is versatile and can be adapted to monitor varying numbers of seedlings at different stages of their life cycle and capture various features and phenotypes from the entire seedling.

For the purpose of evaluating our platform we have considered one commonly studied model organism, *Arabidopsis thaliana* and its genotypes / mutants. We have also chosen gravitropism as our model biological process with its corresponding phenotype being the response of the root. Features of interest chosen are the curvature of the root and the angle of the root tip with the line of gravity.

In a typical experiment, seeds of chosen genotypes are planted in Petri dishes. All the Petri dishes are subjected to identical germination and growing conditions. The Petri dishes are rotated 90^0 (thus altering the gravitational field) and the response of each seedling (the root growth) is observed under a camera. Images are captured at regular intervals (typically varying from five minutes to a few hours between observations). Image processing techniques have been used to analyze the images [19] (in many previous studies manual measurements were performed). The above procedure must be repeated for large populations in order to draw valid conclusions about the biology. This has led to a scenario where the two interdependent tasks namely, data gathering and data analysis, have limited the throughput. Automation of the data analysis is under investigation in numerous labs and is expected to improve efficiency in the analysis, however, the ability to collect data from sufficiently large populations still limits the throughput. The goals of the work presented here are (1) to address issues involved in automated high throughput data gathering and analysis, (2) to set up a system to observe seedlings in a controlled environment, organize and extract data from the gathered images and identify potential phenotypes from the data and to, (3) to analyze the entire system for bottlenecks, pit falls and potential improvements in the system.

The rest of this document is into chapters with chapter 2 providing an overview of the entire system and the work flow. Chapter 3 and 4 describe the hardware and

software of the robotic system. Chapters 5.1 and 5.2 describe in detail the techniques involved in extracting and analyzing features. Chapter 6 analyzes and evaluates the system performance and pit falls. Finally chapter 7 outlines future directions and suggestions for improvements.

Chapter 2

Automated Phenotyping System

In this chapter we outline the pipelined process or the workflow. The workflow describes the steps involved in organizing and scheduling of the planting, imaging and analysis of the seedlings and the corresponding image data. The workflow has been broken down into five principal steps, namely scheduling, preparation, data gathering, feature extraction and data interpretation, which are described below and subsequently described in detail in the later chapters.

2.1. Scheduling

The process of scheduling involves automatically converting the specifications of the plant biologist into

(i) Duration of data gathering experiment.

(ii) Planting and treatment instructions.

(iii) Instruction for organizing of Petri dishes into groups for each data gathering sessions.

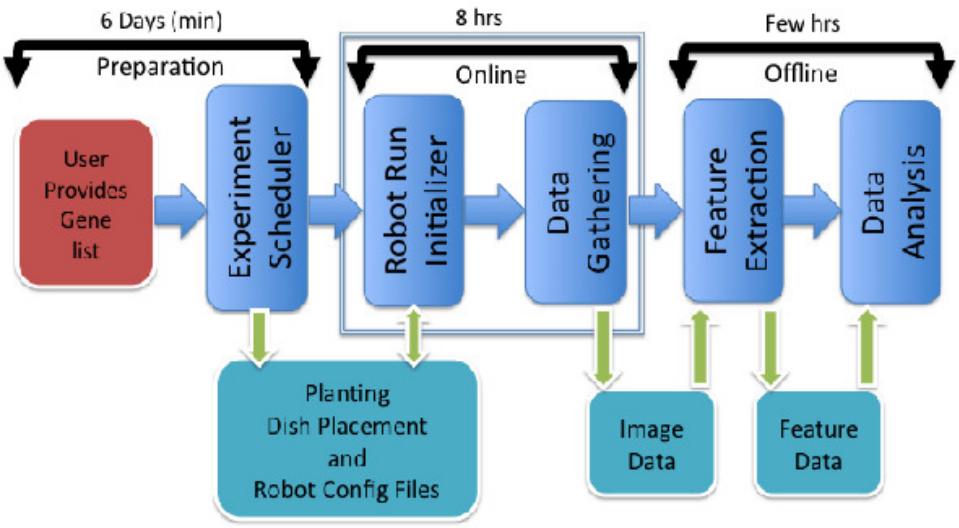

Figure 2.1. Automated Workflow.

(iv) Meta data that will be tagged into the images.

The plant biologist provides a list of genotypes that are of interest and the number of seedlings of each type that need be to imaged. In addition any other information regarding the experimental conditions can be provided. This information is provided as spreadsheet file. The software automatically determines the number of data gathering sessions that will be required and generates a schedule along with planting instructions for each sessions (type of growth media, list of genotypes and their quantity). In addition for each session the program specifies Petri dish placement instructions, and a file for generating labels for each Petri dish. The program also specifies instructions for a few spare Petri dishes that will need to be prepared. Finally, a configuration and meta data file is prepared that is passed to the data gathering program that controls the robotic system. The program, when provided the yield rates (discussed in section 6) from previous runs will adjust the number of seedlings or gathering sessions to ensure that the required amount of data is available to the plant biologists.

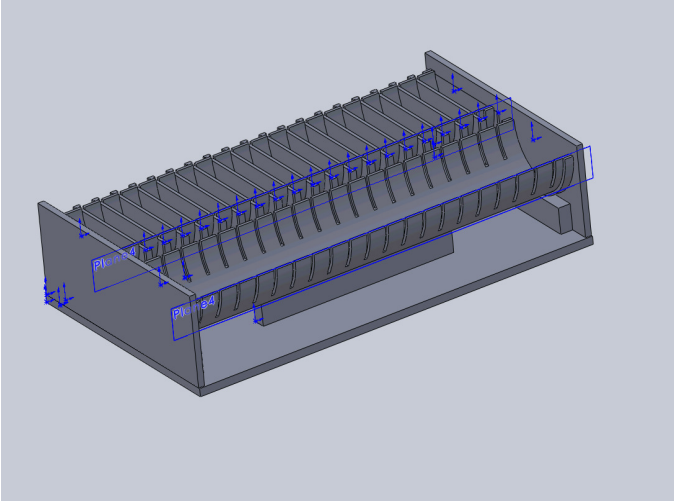

Figure 2.2. Petri holder designed to hold 40, 10cm Petri dishes. The dimensions allow it to be used in a standard refrigerator and growth chamber.

2.2. Planting and Handling

The scheduling program provides the planting instructions for each gathering session. The instruction file contains information about the growth media, treatment and growing condition, genotypes, their quantities and their placement information during their germination and growth. The seeds are planted in 10 cm Petri dishes. All the Petri dishes are then loaded onto a specially designed holder that has the capacity to hold all the Petri dishes required for one gathering session (shown in figure 2.2). The holder allows all the dishes to be easily moved from refrigerator to the growth chamber and to the robot system. The holders are made from clear polycarbonate to allow for uniform lighting and when fully loaded has spaces between Petri dishes to allow airflow to keep the conditions around all Petri dishes uniform, when in the growth chamber. Primarily, the holder firmly grips each Petri dish to prevent it from rolling or wobbling while keeping them upright. This helps reduce the variation in handling conditions between dishes and between data gathering sessions. The holders are designed such that they can be built to accommodate different sizes and quantities

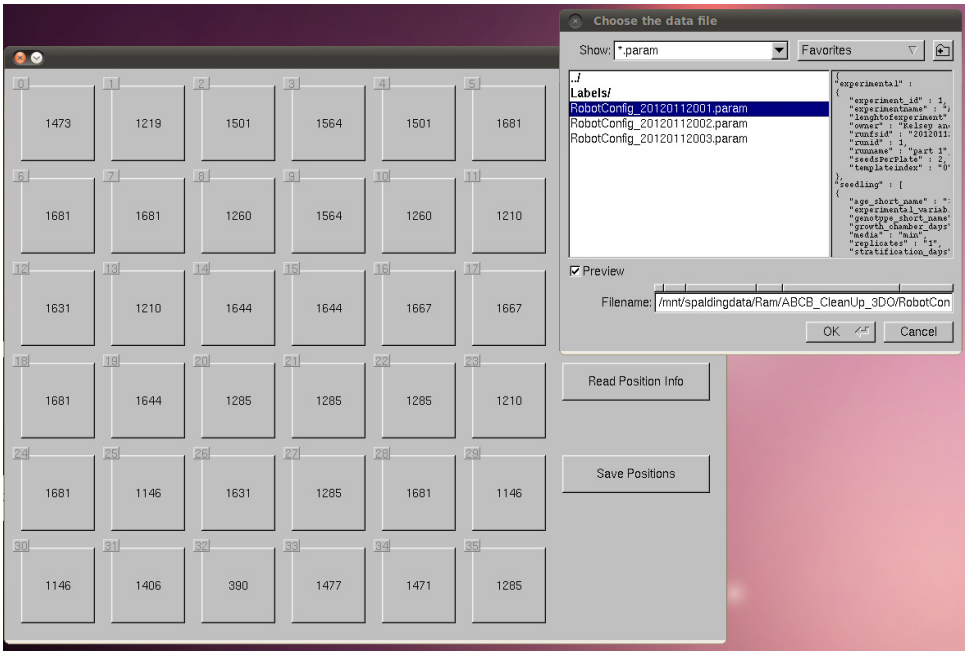

Figure 2.3. Robot Initializer program allows for reassigning Petri dish position prior to data gathering.

of Petri dishes.

2.3. Data Gathering

Once the Petri dishes have been subjected to the specified growing conditions they are ready to be imaged. In some cases the specified Petri dishes may have developed some issues, namely failure to germinate, dislodged seed, etc.. The spare Petri dishes (prepared as specified in the planting instructions) can be used to replace the faulty Petri dish. The first part of the data gathering section consists of the robot initializer program that will allow the operator to quickly update the corresponding files to maintain consistency if a Petri dish had been substituted. A screen shot of the program is shown in figure 2.3.

The second part of the data gathering segment of the workflow consists of the

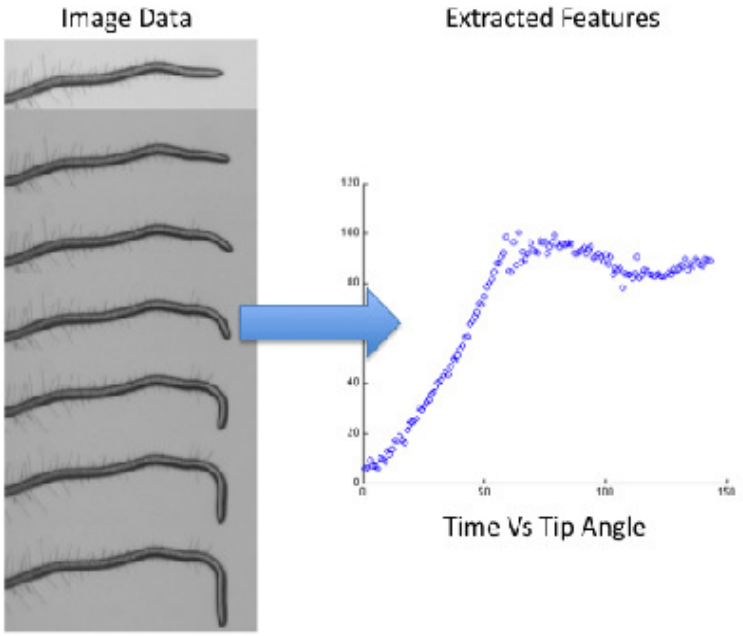

Figure 2.4. Feature extraction steps.

robotic hardware and its corresponding control software that gathers the image data for the time specified by the plant biologist during the scheduling step of this workflow. The robot control program automatically determines the number of time points that will be collected for the specified duration using performance data that is collected during the gathering process. In addition, all meta data (experimental conditions, workflow information, etc.) provided are incorporated into every image that is gathered. Once data has been gathered it is appropriately organized for storage and further analysis. Details of the design of the robotic equipment and the techniques used in its control software are discussed in chapter 3 and chapter 4.

2.4. Feature Extraction

The feature extraction portion of the pipeline takes the stored images and extracts features that are needed to represent or characterize a specific phenotype of interest.

For gravitropic studies the commonly used features are the the angle of the root tip and the curvature of the root, computed at each time point. Typical graphs showing root tip angle and curvature values over the entire observation period are shown in figure 2.4 and 2.5.

2.5. Data Interpretation

Some preliminary data interpretation can be performed automatically on the gathered feature sets to either identify critical features or to perform some form of clustering. Detailed analysis (e.g. quantitative trait loci, QTL) can then be performed once features and time points of interest are identified. The initial analysis helps reduce the complexity and computation time of analysis like QTL. Some initial results using the root tip angle features are discussed in chapter 6.

2.6. Case Study : A Data Gathering Session

This section contains a description of a typical data gathering session and the procedures involved in preparing the seedling, placing them in front of the robotic system for data gathering. The plant biologist prepares the necessary information for the scheduler and obtains all the planting and placement instructions.

Typically, Petri dishes are filled (about 2 to 3mm deep) with agar (a commonly used growing medium) and seeds are planted in a predetermined pattern, to minimize the interference of one seedling with another, then placed in a low temperature environment for 2 days, to induce germination (stratification step). All Petri dishes are loaded onto the Petri dish holders, keeping all seeds in a uniform and controlled growth environment, where the seeds begin to germinate and grow into seedlings. The Petri

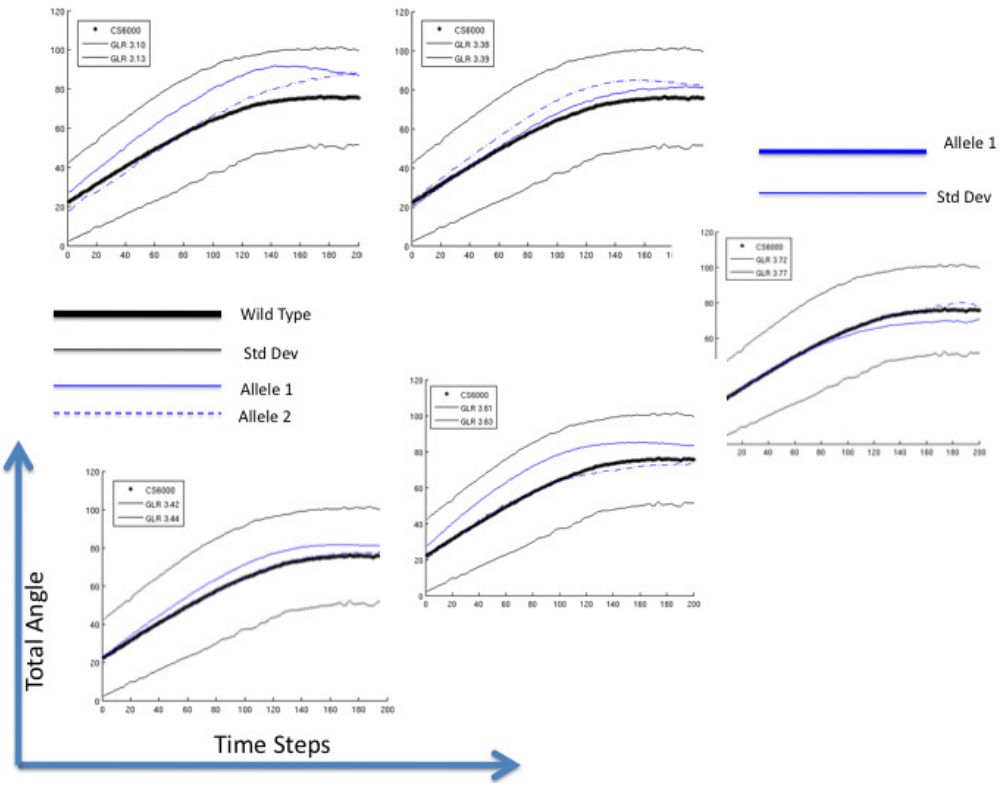

Figure 2.5. Example Plots.

dishes are stored vertically and illuminated from above during germination to force the seedlings to grow straight and vertical. For gravitropic experiments, the Petri dishes are rotated by 90^o so that the seedlings are horizontal (the cassette is rotated to rotate all samples simultaneously), as they are loaded onto the PDCU cassette (discussed in chapter 3). Once the cassette is loaded, the robot visually servos to the root tip and records location containing the root tip. Images of the root tip at these locations are collected over a period of 5 to 8 hours at regular intervals.

The seedling images shown in figure 2.6 have been manually cropped, otherwise all data collection is completely autonomous once the cassette has been loaded. Figure 2.6 shows a time lapse of a single seedling as it responds to gravistimulus (The stimulus provided was the turning of the seedling from its vertical growing position to a

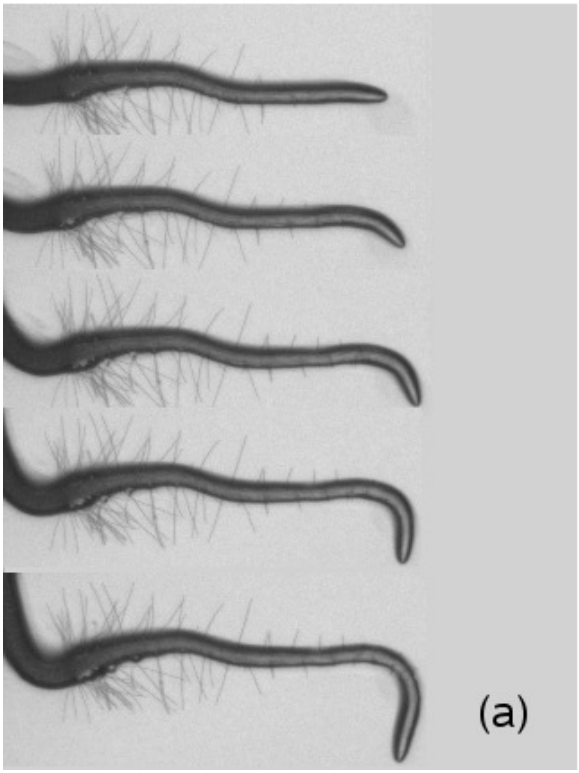

Figure 2.6. Seedling responding to gravistimulus. Each image shows the same root at different time points over a period of 4.5 hours.

horizontal position).

Figure 2.7 consists of two plots overlaid on each other. These plots correspond to the observations of the seedling shown in figure 2.6. The color coded 2-D surface plot shows the curvature measured along a $1mm$ region $100\mu m$ behind the root tip (along the ordinate) at each time point (along the abscissa). Typically the region next to the root tip is of interest to plant biologists and hence the plot only shows the region of interest. The second plot shown (overlaid on the curvature plot) is the curve showing the angle (ordinate) of the root tip (with respect to the horizontal) at each of the same time points. These measurements for this figure were extracted using techniques from [19]. The plot shown here includes only data from a single seedling. Phenotype studies must extract data from a large number of samples for

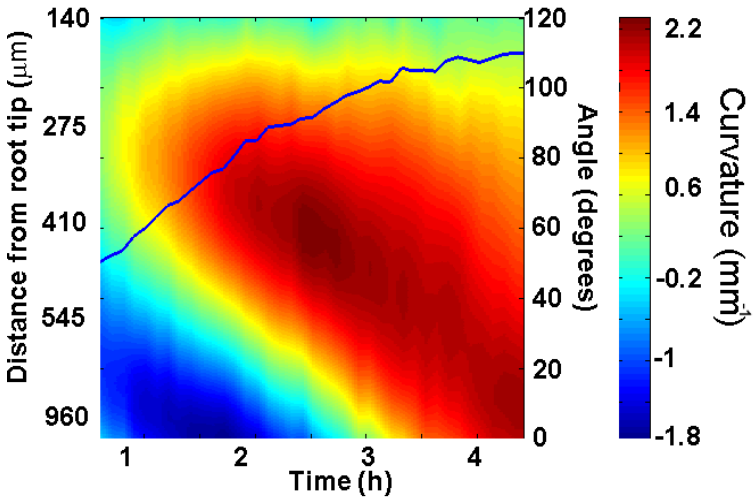

Figure 2.7. The color coded plot shows the curvature of the region of the root close to the tip (within $1mm$). The line plot shows the angle of the tip (with respect to the horizontal) over the same time period.

each mutant type. Further work is required to create an autonomous data analysis system to analyze the data generated from the robotic system, which we discuss as a part of the workflow.

Chapter 3

Robotic System : Hardware

This chapter contains a description of the hardware components of the automated pipeline. Here we also provide a description of the entire design process, starting with the enumeration of the requirements, to the finished system.

3.1. Requirements, Goals and System Specifications

Here we describe the major goals, ideal specifications (for data gathering) based on the nature of the experiment. Section 3.1.1 and 3.1.2 outline the experimental requirements and the ideal specifications needed for an automated system. The final section describes the details of the current robotic hardware and the design of the corresponding fixture to house the Petri dishes. We start by stating the two major goals driving the development of the system.

1. Development of an automated system to increase data gathering throughput in an effort to bring the scale of data gathering closer to that of data analysis.

2. To study the effect of experimental and system parameters on the accuracy and throughput of the system for data gathering.

3.1.1. Experimental Requirements

The requirements of this system were dictated by the size of the seedling and the nature of the experiment. Thus we will first list the specifications of the arabidopsis seedling and the experimental conditions below

a. The seedlings need to be 3 to 4 days old (after germination).

b. As the seedlings are subjected to a gravity stimulus they should not be exposed to any other motion.

c. The seedlings need to be grown vertically (to simulate their growth in soil). During the time of data gathering the seedlings need to be tilted to a horizontal position (to provide the gravity stimulus, which will cause the root to turn towards the direction of the action of gravity).

d. Lighting needs to be consistent for all seedlings at all times during the post germination period and during data gathering.

e. The seedlings are sensitive to all wavelengths of light in the visible spectrum thus imaging will need to be done with strobe lighting or with lighting that has a wavelength lesser/greater than visible spectrum.

Based on the above mentioned seedling description and the nature of the experiment, the specifications for the task at hand are listed below

(i) Increase the data gathering throughput while satisfying the experimental conditions.

(ii) Develop a rig to house seedlings with the required conditions and with consistency, while satisfying the throughput requirements.

(iii) Automate the process of data gathering from the step the the genotypes are specified for imaging to the step when the features are extracted and interpreted.

(iv) Analyze performance of the system in terms of throughput, above mentioned seedling & experimental specifications and methodology used to gather data.

(v) Identify the potential bottle necks to the increase throughput.

3.1.2. Ideal System Specifications

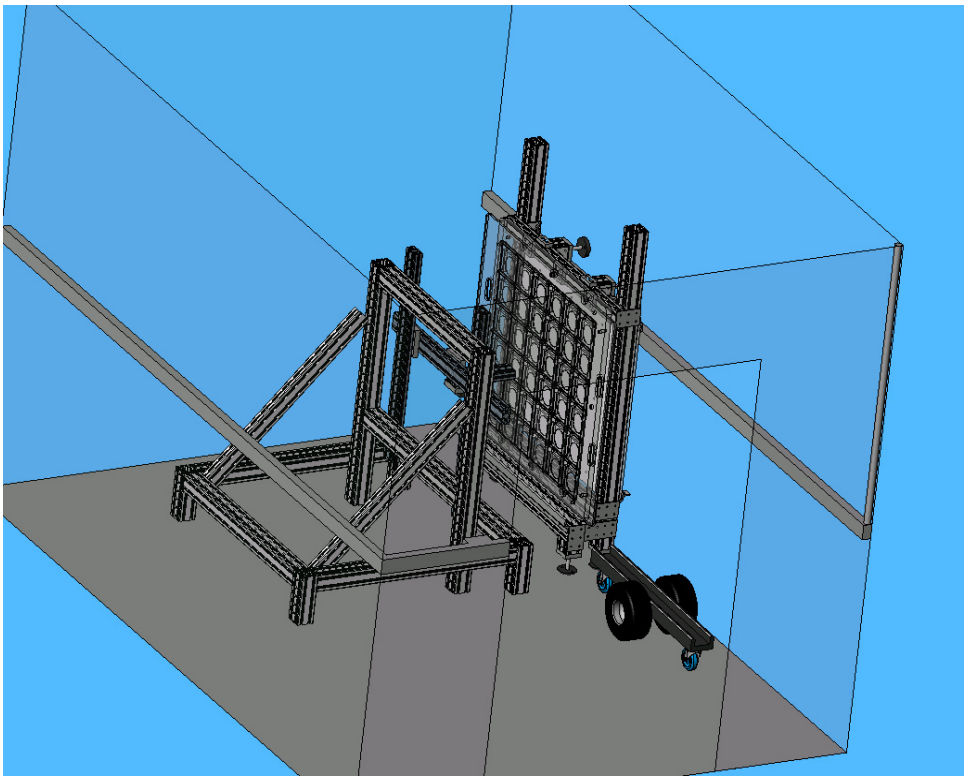

Figure 3.1. Diagram showing the gantry robot and Petri dish holder

The design specification of the robotic system are listed below. They are listed separately for the Petri dish holder and the robotic system. In this section we outline the ideal requirements and simultaneously provide the details of the actual system

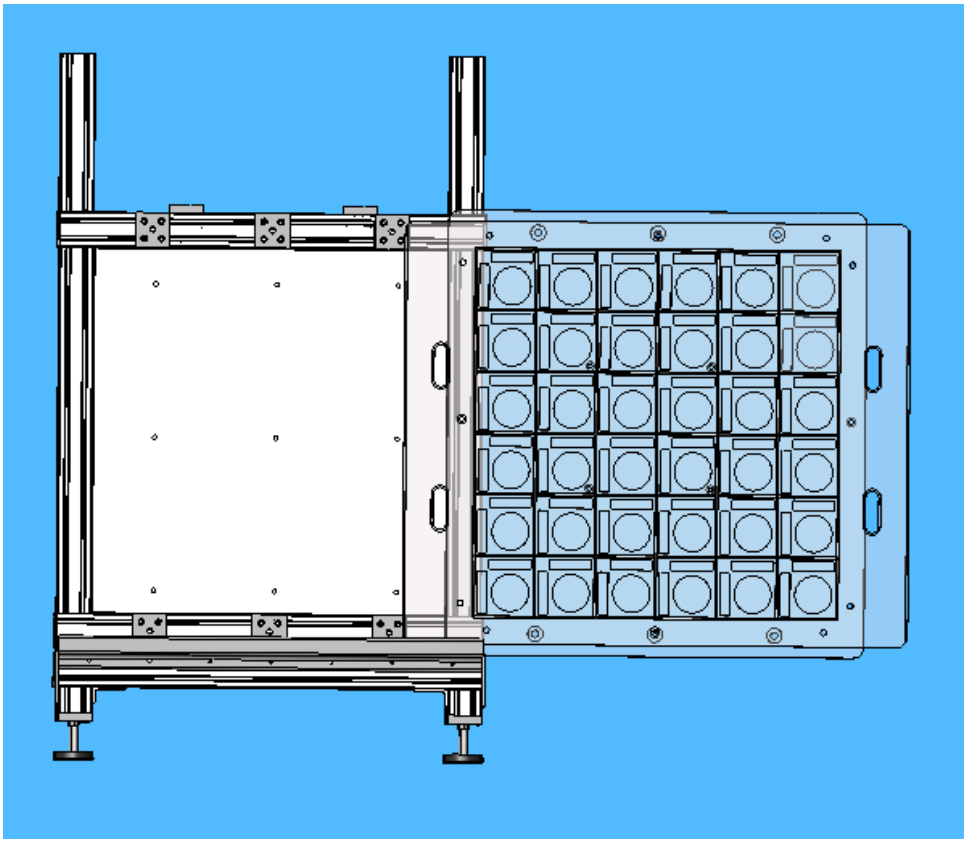

Figure 3.2. Petri Dish Containment Unit (PDCU) Schematic. This schematic shows the Petri dish cassette being inserted into the PDCU, in front of the PDCU infra-red backlight diffuser.

that has been built. More details about each component of the system are provided in section 3.2. In order to have an approximate throughput of about one order of magnitude data acquisition greater than any currently available technique, the Petri dish holder was designed to hold at least 36 seedlings and can hold as many as 700 seedlings (the maximum number of seedlings imaged at high spatial resolution concurrently, thus far, have been about 10 seedlings per session, using 10 cameras observing a seedling each).

Petri dish holder

1. Each unit holding the seedling needs to be illuminated with grow lights and infra

Workspace	x	$1m$
Dimensions	z	$1m$
	y	$0.2m$
Accuracy		$1\mu m$
Repeatability		$0.1\mu m$
Speed		$1m/sec$
Payload		$10kgs$

Table 3.1. Gantry Specifications

red back lights.

2. The growing conditions of each seedling need to be isolated from the others.

3. All seedlings being observed must be subjected to the same gravity stimulus.

4. The device or structure holding the seedlings must be rigid and must not shift the seedlings during the course of data acquisition.

Based on these requirements the Petri dish holder was designed to hold a vertically mounted grid of 36 Petri dishes arranged in 6 rows and 6 columns (further details are provided in section 3.2.1). The specifications of the robotic system listed below are based on the design of the Petri dish holder.

The Robot

1. To allow for variations in planting for different experiments and different seed types the robotic system needs to have the ability to move in and out of the vertical plane. Hence, a workspace of at least $1m \times 1m$ in the vertical plane (a 6×6 grid of Petri dishes occupies an area with a dimension $1m \times 1m$) and $0.2m$ in and out of the plane is required.

2. The width of the root is sub millimeter and the overall length of the root is about 5 *to* $6mm$. Hence, the robot not only needs to move through the $1m \times 1m \times 0.2m$ workspace at high speed from one Petri dish to another, but also move distances of the order of one millimeter with high accuracy.

3. With position resolution reaching the order of microns, much greater accuracy and repeatability values are required. These values may need to be as small as tens of microns.

4. The throughput will depend on how fast the robot can move from one location to another while maintaining the levels of positioning accuracy mentioned above. Each axis of the robotic system should be capable of achieving speeds of up to $1m/sec$.

5. In addition to the above requirements the robot must have the ability to move a payload of about $5kgs$ to support 2 or more cameras and their fixtures.

3.2. System design and description

The goal for high throughput is to increase the number of seedlings observed for a particular phenotype study, provide observations at fine time resolution and to perform these tasks autonomously with consistency and repeatability. The number of seedlings observed can be increased by either (1) increasing the number of seedlings that a single static camera observes, (2) increasing the number of static cameras, as done in [19], or (3) increasing the number of seedlings that each camera observes by having the camera move between Petri dishes. This will allow imaging of the seedlings at any given scale without being limited by size of seedling or the length of the experiment. Using option (1) will increase the throughput at the expense of spatial resolution. Option

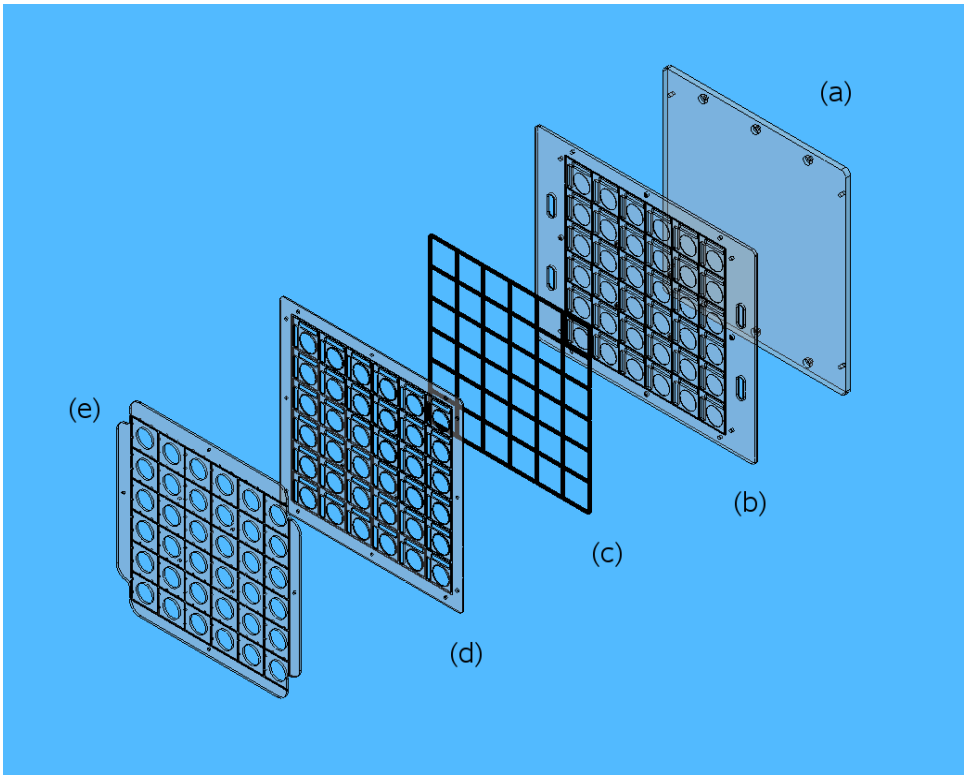

Figure 3.3. Schematic showing an exploded view of the Petri dish cassette. (a) Levelling plate (b) Bottom holder plate (c) Divider Plate (d) Top holder plate (e) Light holder plate.

(2) is a viable option, but managing large arrays of cameras can become complicated and expensive as the throughput increases. Hence, we choose option (3) to increase seedling throughput without compromising on spatial resolution. Table 6.1 provides some comparisons between the three methodologies.

In this section we describe the prototype system which consists of two major units, the Petri dish containment unit and the gantry robot. The Petri dish holder provides a fixture for the plant samples, while the robot moves the cameras to acquire images of the seedlings. The computer aided design drawings, spec sheets and manuals for all the components are available but have not been included in this document.

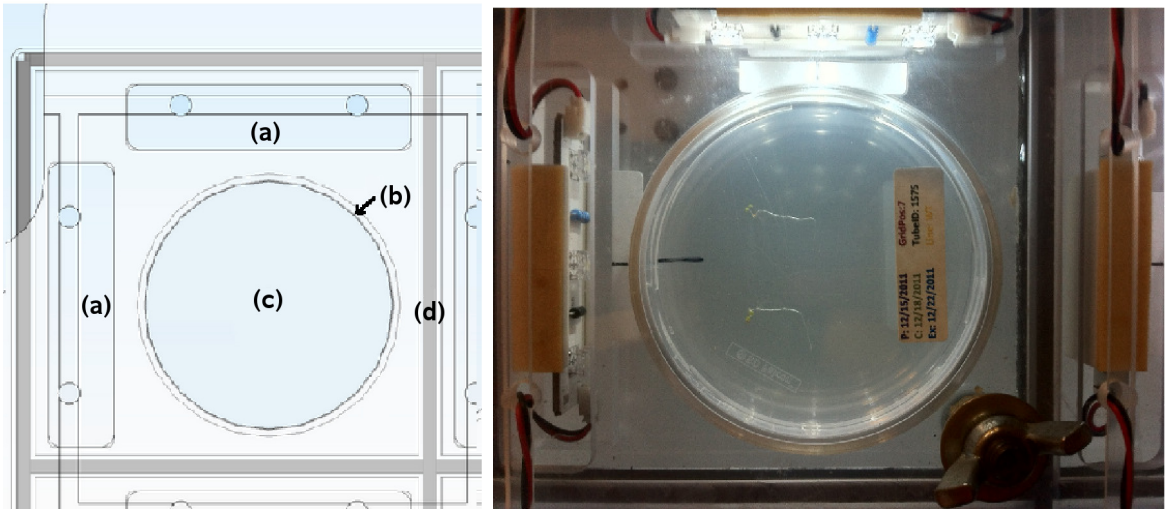

Figure 3.4. Schematic and corresponding image of a single Petri dish in the PDCU. The components labeled are: (a) LED grow lights (b) Petri dish (c) IR backlit region (d) Separators (dividers) that isolate each Petri dish

3.2.1. Petri dish containment unit (PDCU)

The Petri dish containment unit was built adhering to the specifications discussed earlier in this chapter. It holds 36 Petri dishes in a grid pattern as shown in figure 3.2. This unit consists of a removable cassette and a fixture (frame) to hold the cassette in place (see figure 3.2). The fixture has been built with extruded aluminum parts obtained from 80/20 inc. This fixture has a set of pads that allows for adjustments and anchoring to the floor and wall. Once adjusted to be vertical and level the fixture is anchored and is never moved. The Petri dish cassette can now be inserted and removed repeatedly without causing any change in position. The infra red imaging lights are located behind the levelling plate. The infra red lights are a set of infra red light emitting diodes (LEDs) located in the regions directly behind the Petri dishes. The LEDs are covered with a diffuser sheet for uniform back lighting and reducing blooming effects. Figure 3.3 shows different parts of the PDCU. Figure 3.3a is the levelling plate that is permanently mounted on the fixture. All levelling adjustments

to the fixture are performed with respect to this plate (when in place the cassette is flush with the levelling plate). The bottom holder (figure 3.3b) is machined with circular pocket to hold the Petri dish base while the top holder (figure 3.3d) holds down the lids of the Petri dishes. The divider plate (figure 3.3d) is a grid of separators that isolate the environment around each Petri dish and its lighting. The light holder holds all the growth lighting required. These are housed on a separate sheet so that they can be swapped based on experimental specifications. All the plastic sheets are held together with bolts and wing-nuts. The bolt locations were chosen to minimize cassette flexure. These plates were designed to hold the Petri dishes in place by a compression fit to prevent any shift in location of the Petri dish over time (when standing vertically).

The Petri dishes are loaded onto the cassette vertically (6 rows by 6 columns). As the robotic system is able to move the camera, each dish can contain multiple seedlings, initial tests have been performed with 4 seedlings per Petri dish. Every Petri dish location (shown in figure 3.4) is equipped with its own growth light and is isolated from the other Petri dishes (using opaque partitions) to ensure uniform lighting conditions. When the whole cassette is secured onto the fixture it is illuminated with an IR back light. The primary purpose of the back light is for illumination during imaging, the wavelength of the IR lights are chosen to minimize interference with the growing patterns of seedlings. The whole Petri dish containment unit is designed to be modular, all lighting (both grow lights and back lights) can be swapped out for various experimental conditions. For gravitropic experiments, two sets of lights, aligned at 90 degrees from each other are used for each Petri dish. Initially one set of lights are used during germination, and after rotating the holder, the second set is used during imaging. Thus the seedlings are uniformly lit from above (to mimic natural growing

conditions) for the entire duration of their germination and data gathering.

3.2.2. Gantry Robot

The specification of the robotics system as described in the preceding sections posed a big challenge. The primary problem was that no off-the-shelf robotic system could be used. The constraints on the speed, accuracy and work space, which by nature are counteracting, were extreme. Off-the-shelf robotics systems satisfied a subset of the specifications. E.g., systems that could achieve speeds of $1m/s$ could not provide micron level precision in positioning while handling large payloads. Tests using robots with sub-millimeter positioning precision operating with maximum limit payloads resulted in substantial increase in their position error. Those that handled large payloads with high precision could not provide the high speeds, while others could not handle the large workspace requirement. Thus a custom system needed to be designed and built to meet all the stated specifications.

The gantry robot was constructed with help from Intellidrives Inc. based on all the design criteria discussed in chapter 3.1.2. The robot has 3 axes of motion and is fitted with 2 cameras, all axes are powered by linear servo motors. The robot has a workspace large enough to servo the cameras along the vertical (x-z) plane to all positions of interest in Petri dish cassette. The dimensions, positional accuracy, and other specifications are listed in table 3.1. Each axis uses a direct drive linear servo motor. Linear servo motors were chosen over the screw type and belt drive systems primarily due to the simplicity of construction, better position resolution & repeatability and the large workspace requirements. One 4-axis master PID controller is used for global control of gantry. The master controller connected to the control computer via ethernet (see figure 3.6). The linear actuators used for the x and y

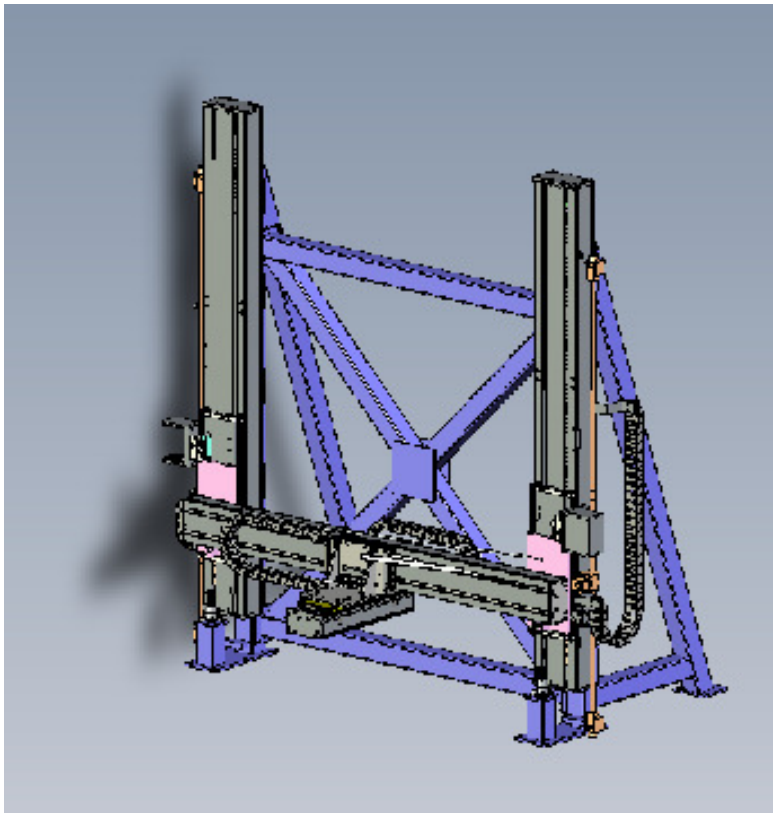

Figure 3.5. Schematic of the 3 Axis Gantry Robot

axes are the *LSS-160* units, while the ones used for the z axis were the *LSS-200*, table A.3 provides specification details for each axis. The drives for each axis were the Xenus line of digital servo drives sourced from *Copley Controls Inc.* The x and y axes use the *XSL-230-18* and the z axis uses the *XSL-230-36* models. The z-axis drives are equipped with regeneration resistors to protect the amplifiers from a voltage overload (this may occur due to excess back emf build up if the x-axis drops and the z-axis brakes fail or are disabled). The 4-axis master controller was sourced from *Galil Motion Control Inc.* and the model used is the *DMC-4040* motion controller. A schematic of the complete system showing how the different components interact is shown in figure 3.6.

Currently two cameras are mounted on the end effector of the gantry, shown in

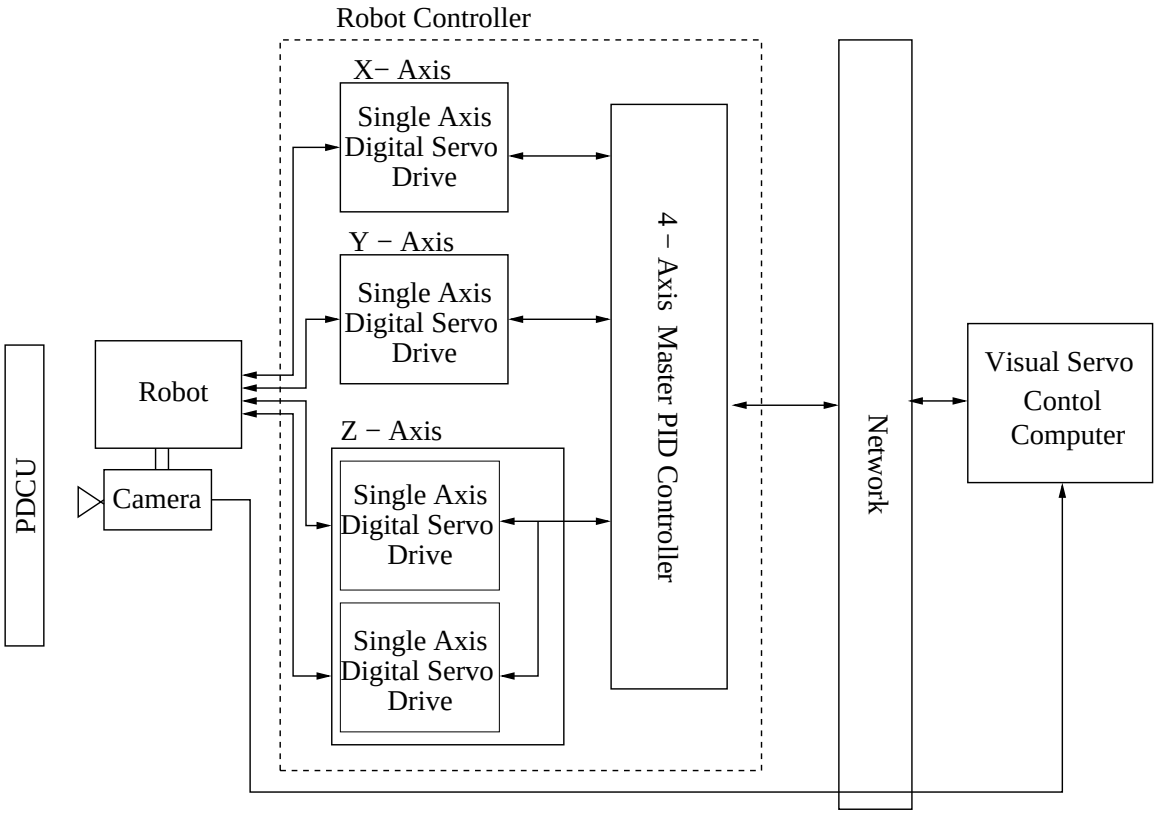

Figure 3.6. Schematic of the Robot Control System

figure 3.7. Camera 1 with a low magnification lens is used for determining seed location and camera 2 with a high magnification lens is used for servoing and image gathering (Both cameras are calibrated). Camera 1 captures images illuminated with the white grow lights. Camera 2 captures images illuminated with the IR backlight. The PDCU provides a fixture and ideally a simple calibration would enable the robot to monitor each Petri dish. However, the optics used for image capture have a restricted depth of field, and the seedlings move during germination and growth. To ensure the sample is within the field of view, and in focus, we use the vision system to track the root and center the tip in the field of view. The following chapter presents, in detail, this task that the vision system needs to perform. Also provided is a brief outline of visual servoing, which is the technique adopted to control the robotic hardware

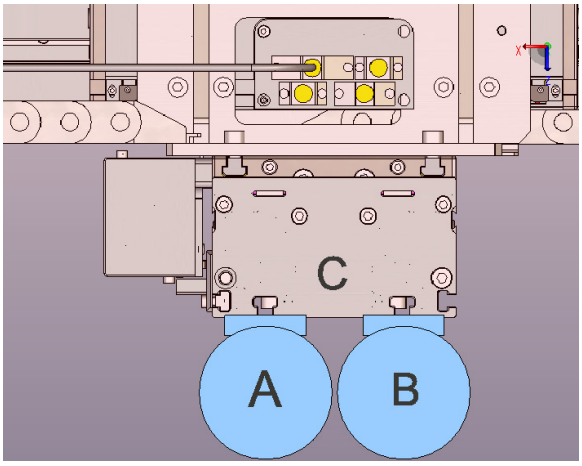

Figure 3.7. A diagram of the two cameras installed on the end effector. (A) Low magnification camera and lens. (B) High magnification camera and lens. (C) Robot end effector.

using the image information as a feedback system. A detailed discussion of the image processing techniques developed for servoing, camera focusing and identifying the features of interest in the image are described in the following chapter.

Chapter 4

Robotic System : Software

In the previous chapter a description of the robotic hardware and construction of the PDCU was provided. The following section discusses the technique used to control the robotic system and to collect images of all the seedlings planted in the PDCU. The collected images will provide time series information of each seedling during the course of an experiment. Currently, all experiments involve the observation of the seedling's (root tip) response to a change in gravity stimulus.

To collect image data concurrently the robotic system needs to determine the precise location of root tip of each seedling. An initial attempt to determine root tip locations was carried out by (a) planting seeds at preset locations within the Petri dish and (b) moving the robot to the predetermined locations (taking into account approximate size of the seedling and location within the Petri dish and PDCU) to estimate the location of root tip of each seedling. This approach was quickly abandoned as the effective yield of usable seedling image data was well below 50%. Additionally such a technique would also require rigorous position calibration and would not generalize well to image other species of plants or other phenotypic information from the

seedlings.

Presently, the strategy adopted involves planting the seeds in a predetermined pattern (in the Petri dish), rapidly positioning the robot to these predetermined locations. This should bring the low magnification (large field of view) camera into the vicinity of the location to image the planted (in the Petri dish), i.e. the seedling is located within the large field of view. Subsequently the robotic system switches to use the high magnification camera and follows the root (of the seedling) to the root tip. The search for the seedling and the root tip are performed using visual servoing. A search for the seedling has to be performed as the seedlings are not guaranteed to be at the exact location that the seeds are planted due to small amounts of drifting (the list of problems and failures are discussed in detail in sections 6.3.2 & 6.3.1). The root tip's have to be located to monitor the changes in the phenotype. In addition to a spatial search in the image for the seedling and root, a search for the *best focused* image is required. This is done to maximize the quality of the image data gathered. As the camera lenses used are fixed focal length lenses, the only available strategy to adjust focus is to change the position of the lenses to move the focal plane (depth at which the lens is focused) by moving the cameras in and out of the plane of the PDCU (normal to the plane of PDCU). The following sections provide discussions of the image processing required for visual servoing to the root tip and servoing for the best focal plane.

4.1. Visual Servoing

Visual servoing is the process of actively positioning a robot using visual information as feedback for position error correction (with respect to a target location or a desired robot configuration). Briefly the process of visual servo control is explained

with the simplified algorithm below

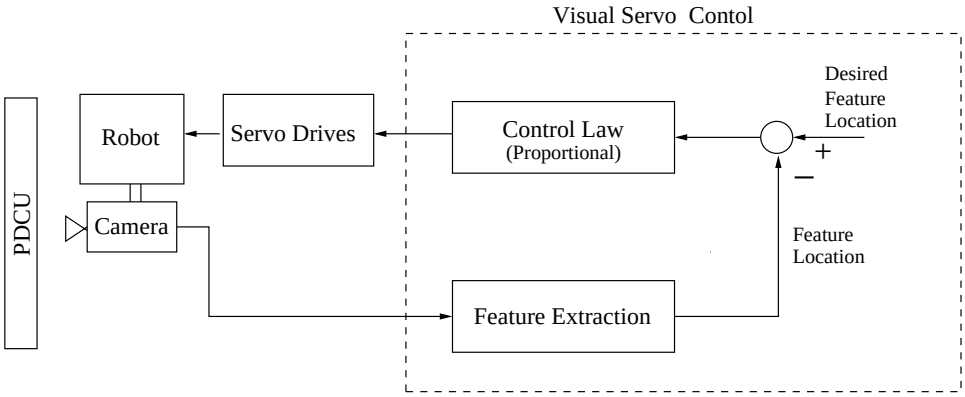

Figure 4.1. A typical visual servo control loop.

(1) An image is obtained from the camera.

(2) *Interest points* are identified and a target is defined.

(3) An error is defined based on the closeness to the target.

(4) To minimize the position error a decision to move is made (typically as a pose or as a set of translations and rotations).

(5) Repeat until an *end condition* is met.

We use the above visual servo control outline to highlight a few critical points. The term *interest points* (good features, or landmarks) is very loosely defined in the visual servoing literature [27, 4, 18]. Most previous work assumes that *interest points* are explicitly marked points in the image. Some, more recent work have used image regions (image moment information) as *interest points* [1, 4, 30]. In addition, prior work on visual servoing assume that *interest points* are always available in the obtained image.

Preliminary tests were conducted by using artificial markers in each Petri dish. This introduced an extra manual step in the preparation process and in the addition

of a new set of challenges. E.g. the growing medium can be of varying depths, which would require adjusting the camera focus to find the markers. The problems are further complicated as the depth of focus is very small (approximately $1 - 2mm$). Hence we chose to analyze the image to extract naturally occurring features as markers or *interest points* namely the seedling (root). This approach has an added advantage as it can be used as a pre processing step when phenotype information is extracted from the image. The segmentation of the root from the image forms the critical step of the visual servoing loop and determines the motion of the robotic system (in the present case the gantry system undergoes pure translations). In our case we need to determine the location of the seedling and the root tip (i.e., we do not know the location of the target).

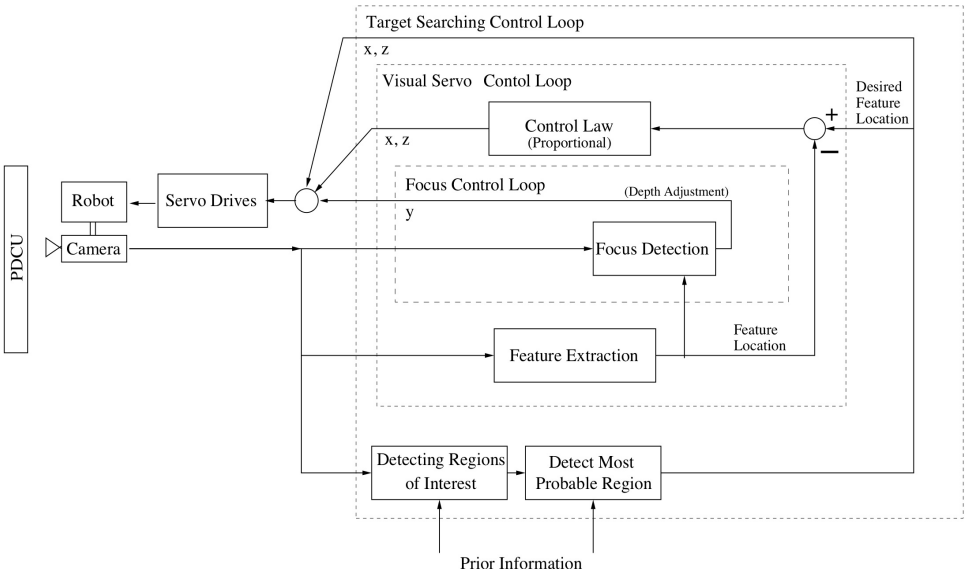

Figure 4.2. The modified visual servo control loop that allows the decoupling of the servoing in X-Z plane and the Y axis. This allows for independent root tip search and focusing.

To alleviate the problem of defining an error metric when the location of the root tip is unknown the servoing algorithm is modified to track along the root until a root tip is detected (i.e. end of root) in the field of view. Once the root tip is determined

Figure 4.3. An image of a seedling root responding to a change in gravity stimulus

to be in the field of view a conventional image based visual servoing algorithm [11] is used to center the tip in the image. Additionally, as we have a small depth of field we may not have the root or seedling in focus and may not be able to servo to the root tip. Hence a focusing step has to be performed during the servoing process or the technique should have the ability to process images even when out of focus. Thus the segmentation technique would have to be developed to work with images that may be out of focus. The following sections discuss in detail the technique and provide an analysis of its performance. Figure 4.2 depicts this modified servo control loop. The modified servo loop allows for independent control of the axes, i.e. the search for the seedling can be carried out independent of the search for the focal plane. The following sections describe the segmentation technique for visual servoing and the algorithm used for focusing.

4.2. Image Processing for Visual Servoing

4.2.1. Identifying the root and root tip

From an image processing standpoint methods need to be developed (a) to identify the root in a given image when guiding the robot motion (b) to determine the root tip to define a location to be visited repeatedly to obtain the time lapse images of the root's response to gravity, (c) to analyze the collected images by segmenting the root and converting the image region to a form that allows measurements to be extracted, and, (d) extraction and tabulation of the phenotypic information. Currently parts (a) and (b) are performed on-line while part (c) and (d) are off-line operations. We propose a unified approach to operations (a) and (c) and provide a detailed discussion in section 4.2.1. Also, we aim propose a solution that will generalize to identify other parts of a seedling (for a variety of species) in order to have a versatile system.

The primary challenge that had to be addressed was to reliably locate the seedlings in the Petri dish. In previous work related to image based phenotype analysis segmentation operations and measurement extraction have been able to preset the location of the feature of interest to always lie in the field of view (in some cases, e.g. [2] a location is provided manually). The assumption is valid as the experimental setup is static. These image acquisition systems require manual setup and tuning for each time lapse image stack. In [32, 19] the authors reduce manual effort by bringing more seedlings within the field of view. This is done by either reducing the spatial resolution or bringing many seedlings very close together, introducing a new set of complications caused by seedlings crossing over one another. In our case, a strategy needed to be developed to locate the seedling when it was not within the field of view and automatically adjust the camera position and focus accordingly. The camera is

moved through a fixed region around the initial location and the location with highest rootness (defined in 4.2.1) value is used as the location with a root.

Problems that arise in this task include variations in image intensity, seedling drift, varying types of roots, scratches on the agar and/or Petri dish (which resemble a root). Because of the resolution required for measurement of subtle changes in the seedling, the imaging system has a very small field of view and depth of focus which makes the task of visual servoing more complicated. Figure 4.4 presents some typical images that the vision system encounters. Once the robot has completed the servoing task and performs a focusing step most seedling images resemble figure 4.3. The following points were the list of constraints and challenges that needed to be considered to develop the image processing techniques :

(a) The field of view is approximately $4mm \times 4mm$.

(b) A seedling may not be in the field of view as seedlings can shift as they germinate.

(c) A seedling may not have germinated.

(d) Condensation build up can change image contrast and add noise.

(e) The image can be out of focus (the depth of field is approximately $2mm$).

(f) Scratches on the Petri dish or growing medium often resemble a root.

(g) The depth of the growing medium may change based on length of imaging session and nature of experiment.

(h) The growing medium and Petri dishes are all transparent.

Because the camera may not be focused on the root, or a root may not be present in the field of view, a deterministic technique to find a root in a given image can

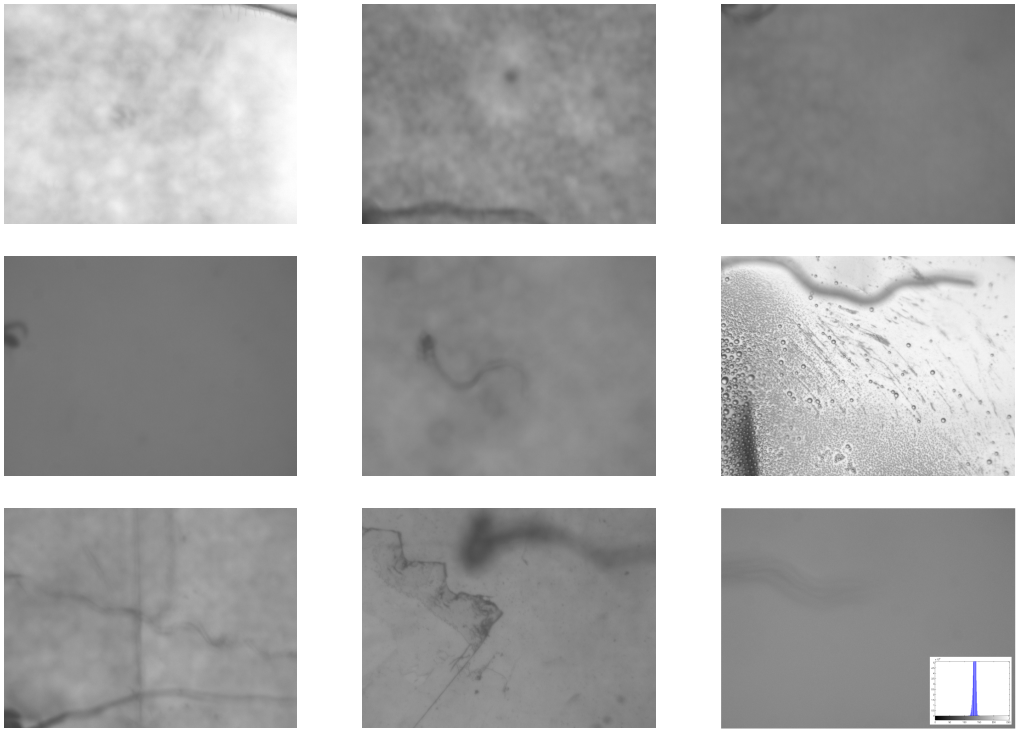

Figure 4.4. These images depict some of scenarios observed when performing the task of visual servoing. In contrast with the "ideal" image shown in figure 4.3, these images present challenges for identifying the root.

prove to be very difficult. The images shown in figure 4.4 depict some of the scenarios mentioned above that need to handled. In addition, the on-line component of the algorithm needs to be very fast (to minimize the time taken to servo to the root tip) to maintain a high data gathering throughput. The following section provides a detailed description of root segmentation procedure. The segmentation task has been split into two operations. The first operation identifies regions of the image that can contain the root. The second operation uses heuristics and probabilities to identify the region with the highest amount of *rootness*.

4.2.1.0. Per Pixel Probability Assignments

Each pixel in the image is assigned a probability using a Bayesian framework. The probability assignments make two assumptions

(a) The root is darker than the background

(b) The root occupies around 3% of the entire image.

The first assumption is because of the imaging modality. The root is not only non-responsive to IR light but is also opaque to it. Thus produces an image with root region containing darker gray levels and other regions with brighter gray levels. The second assumption was determined empirically and is based on the magnification of the lens being used, the field of view available, and, the typical size of the arabidopsis seedlings.

These two assumptions help define the *likelihood* and *prior* terms in the Bayes equation. We define these terms and the probability assignments in formal terms below. We use a single channel image I, of size $m \times n$, with pixel intensities at pixel location x, y

$$I(x, y) = g \tag{4.1}$$

where

$$x \in [0, m-1],\ y \in [0, n-1],\ \text{and}\ g \in [0, 255]$$

We can estimate the probability of the occurrence of g as the frequency of occurrence of g in the histogram of I.

$$p(g) = E(g|I) \tag{4.2}$$

The probability of finding a root in an image based on its relative size in the image, $p(r)$ is 0.03. This value was estimated empirically from a collection of images of the root acquired *a priori*. This value is required to help bias our probability estimate. The final probability assignments are not very sensitive to this value, section 4.2.2 discusses the sensitivity of final segmentation to $p(r)$.

Finally we describe the likelihood function, that will estimate the probability of a pixel belonging to the root having a gray level g, based on our first assumption can be written as

$$p(g|r) = \begin{cases} 1 - \frac{g}{g_{avg}} & : \quad g \leq g_{avg} \\ 0 & : \quad g > g_{avg} \end{cases} \tag{4.3}$$

where $g \in [1, 255]$. We do not include the value $g = 0$ because we use it to test if an error occurs during image capture. If the image is completely dark an error may have occurred, e.g. the backlights may have failed or an erroneous position command was generated causing the robot to move to a position with out lighting or a seedling. The linear function was chosen for its simplicity, a non linear model may have a better approximation of the actual likelihood function but the linear model provides a close approximation.

Using the terms defined above for the *priors* and the *likelihood* we can compute the conditional probability $p(r|g)$, probability of a pixel, $I(x, y)$, belonging to the root given it has a gray scale value g

$$p(r|g) = \frac{p(g|r)\, p(r)}{p(g)} \tag{4.4}$$

Once the probabilities are assigned for each pixel we construct a probability matrix with each entry containing the probability of the pixel in the corresponding location in the image. This matrix is used in the next stage to identify the root.

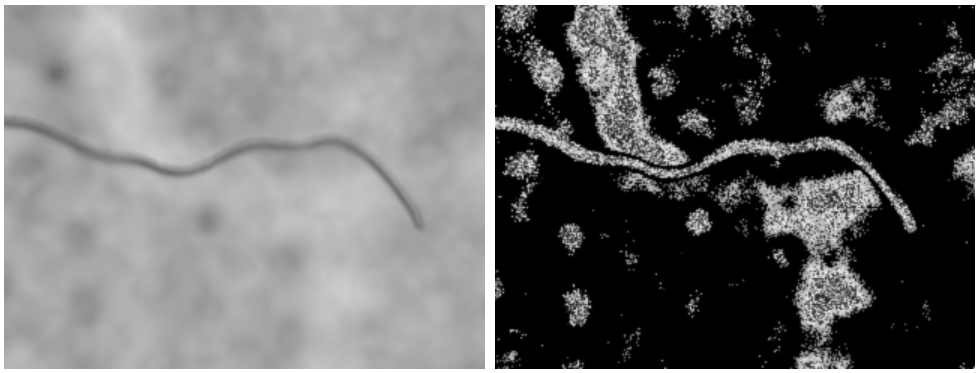

Figure 4.5. The images show the output of the different steps in the segmentation process. (a) Original Image (b) Pixel Probability Image

4.2.1.0. Heuristic Root Selection

From the previous step we obtain a probability matrix. From the original image we remove all pixels with $p(r|g) = 0$. The remaining pixels cluster together forming patches in the image. In images with good contrast the pixels form just one patch. This patch is considered to be the region which best represents the root. In cases with poor image quality many patches are formed. Poor image quality is a result of factors highlighted above. At this stage numerous techniques to exclude *unwanted* pixels can be used. From analysis performed we note that any adaptive threshold technique will work to isolate the *high probability* regions. A fixed thresholding technique works only in some ideal cases. For our purposes we choose to remove pixels that have $p(g) \cdot p(r|g) > p(r)$. This follows from the fact that background pixels will be present in large numbers. The object of interest, the root, occupies a very small portion of the image. Hence pixel intensities that represent large regions can be removed as regions that can potentially contain the root. The removal of these pixels produces isolated regions in the image from which the region containing the root needs to be identified. Section 4.2.2 provides a brief discussion of algorithms' sensitivity to the value of $p(r)$. Each patch is assigned a probability equal to the average of all the

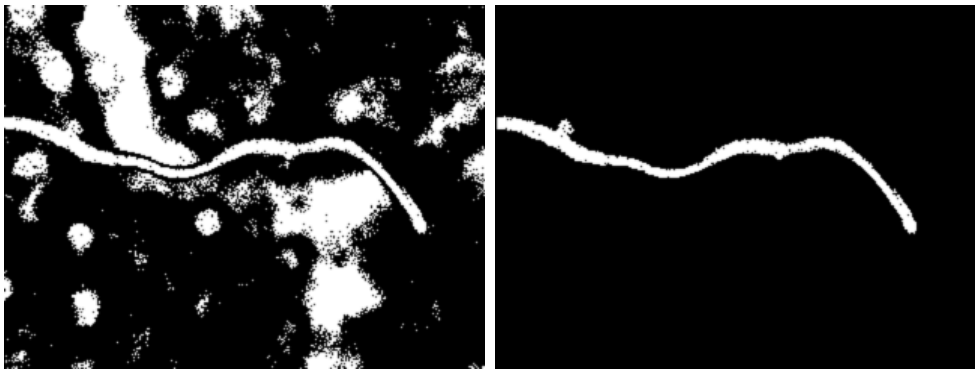

Figure 4.6. The images show the output of the different steps in the segmentation process. (a) Binarized Image (b) Segmented Image

pixel probabilities. Heuristic driven weight assignments are made to each patch. The heuristics use information from basic moment analysis (area, major, minor axis) on the patches. The larger, longer and thinner patches that are more horizontal are weighted higher. We term this weighted probability the *rootness* of the patch. Finally, the patch with the highest *rootness*, weighted probability is chosen as the most likely root patch. If there are n patches in the image we can formally define the *rootness* as

$$w_1^i = 1 - \frac{minor\ axis^i}{major\ axis^i}$$

$$w_2^i = 1 - \frac{Orientation^i}{90} \tag{4.5}$$

$$w_3^i = \frac{area^i}{\sum_{i=0}^{n} area^i}$$

For every patch i, we average the probability over all m pixels

$$p^i_{avg} = \frac{\sum_{j=0}^{m} p(r|g_j)^i}{m} \tag{4.6}$$

$$p^i_{root} = w^i_1 \cdot w^i_2 \cdot w^i_3 \cdot p^i_{avg} \tag{4.7}$$

$$rootness = \max(p^i_{root}) \tag{4.8}$$

The patch designated as having the maximum *rootness* is used for servoing the robot. The robot servos to the tip of the patch (bringing it to the center of the field of view). If the root does extend beyond the field of view, the robot servos until a tip is reached and tip remains near the center of the field of view.

4.2.2. Assessment of the Root Segmentation Technique

The performance of the root segmentation technique was measured by the number of *successful* root and root tip detections while handling all the constraints mentioned in section 4.2.1 as effectively as possible. A seedling was deemed *successfully* detected if the root was correctly found and the servoing positioned the root tip at the image center of the image (within a 100×100 pixel window). Table 4.1 provides the information on the success rate. From the table we note that the system detects the root and is successful 87.4% when a root exists. It is harder to determine the false positive, this is because the region with the most rootness will be detected and in the case when no root is present, the region with the highest rootness will be used. We allow this to

happen as we are not enforcing a hard threshold on the minimum rootness value that we expect for a root region.

The failures were of two kinds, (a) errors in segmentation or tracking or (b) missing seedlings. The segmentation errors were caused by incorrect identification of the root. Errors of type (b) are due to external factors, such as seeds that do not germinate, roots that grow out of the plane of the Petri dish, etc. These seedlings are excluded from the success calculations. Errors of type (a) are caused because the image quality is poor.

We performed a comparison of the output of probability based segmentation technique with segmentation based on the thresholding that used a standard implementation of Otsu [25] to determine the threshold. Some of the results are shown in Fig 4.8. From the images in Fig 4.8(a) we see that histogram is uni modal and thus do not expect Otsu to perform very well (as the primary assumption in the Otsu algorithm is that the image is bimodal, as with many other automated thresholding techniques). But we see that as image quality improves Otsu performs well (e.g., row three in Fig 4.8). We notice similar results when using the Canny [3] edge detector. When using the Canny edge detector on cleaner images (better quality) it is possible to obtain usable results, however the parameters will need to tuned for each image. Fig 4.3(c) and Fig 4.7 shows the output of the edge detection, using Canny, with hand tuned input parameters (sigma of the smoothing kernel and threshold). The output degrades when using fixed values for all images and as the image quality varies.

Section 4.2.1 introduced the use of the prior term $p(r)$. This term was obtained empirically from 300 clean images. Because this value is used as a threshold (of sorts) we tested the sensitivity of the output to it by varying the value of $p(r)$ from $0.02 \rightarrow 0.10$ with no significant change in the segmented image, when image quality was good.

Figure 4.7. Output of Canny edge detector when manually tuned for the image.

When the image quality was very poor (i.e. out of focus or containing scratches, condensation etc.) the value of $p(r)$ had to kept within the range $[0.027, 0.05]$. The increase in sensitivity to the value of the prior was due the shifting of the histogram towards the lower gray values, as the poor images had lower $g_{avg} = E[g]$. In addition the histograms of the poor quality images were spread out over larger ranges of gray levels especially when images were extremely out of focus. For the likelihood function $p(g|r)$, we assumed a linear modelwhich is given in equation (4.3). From the equation it can be noted that highest probabilities are assigned to the darkest gray levels and the value decreases monotonically until the mean gray level of the image. All other gray levels are assigned a zero value. Ideally, a model based on the histogram information of numerous sample images of the root can be built. Other models with exponentially decaying trends were tested, but the model in equation (4.3) is simple and we found that it worked equally well.

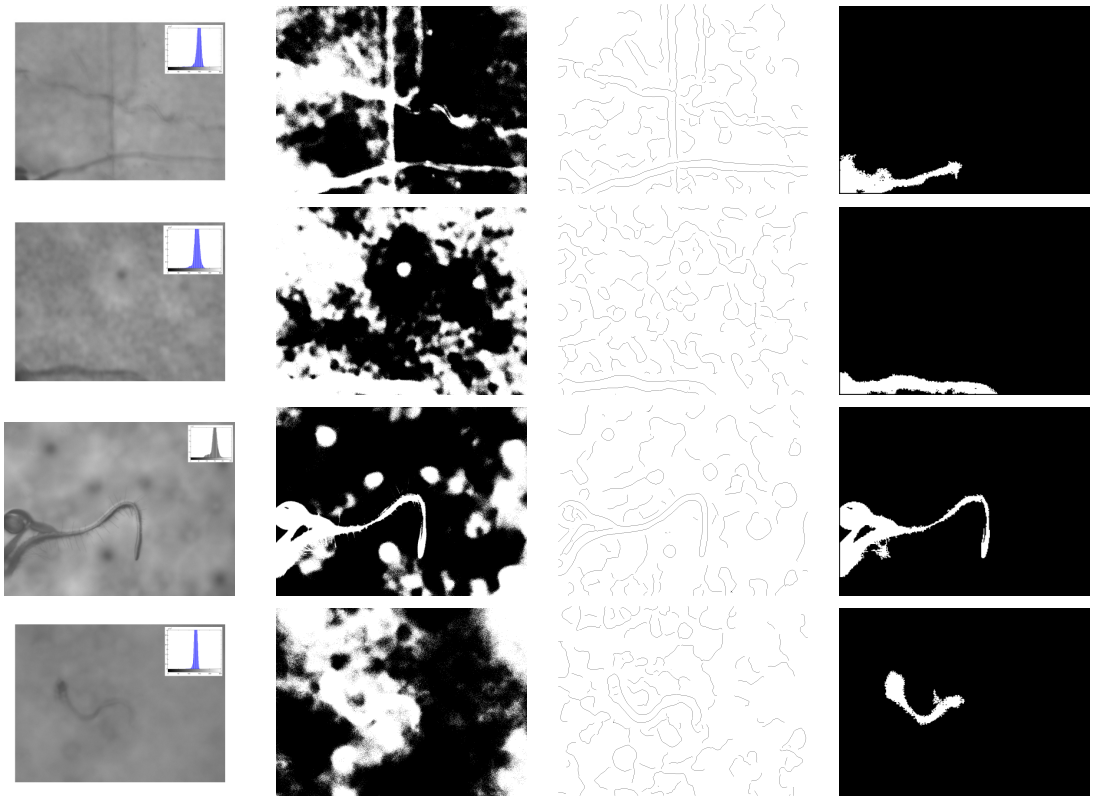

Figure 4.8. The images show the difference in output between the probabilistic approach and a standard implementation of a thresholding algorithm, e.g. Otsu. (a) Original image captured, (b) Output of thresholding when using Otsu algorithm to automatically estimate the threshold value, (c) Output of Canny edge detector when manually tuned for each image (images do not have the same parameter values), (d) Output from the probabilistic segmentation technique

4.2.3. Focusing

Auto focusing techniques fall broadly into two categories, active and passive. Active focusing techniques rely on additional sensors like, lasers, SONAR, etc., to provide additional range information. While, passive focusing techniques employ software based techniques to obtain the same range information directly from the image. Typically, multiple images are obtained and a quantitative measure (focus measure) of the

extent of focus (or defocus) is computed from the image. In both cases a search will need to be performed to determine the location of the best focused image. In our case, we chose to use a passive focusing technique, to avoid using any additional sensors or equipment being added to the gantry.

In the description of the segmentation algorithm (section 4.2.1) we have shown that the servoing can be performed with images of the root that may be out of focus. This section describes the technique used for searching (along the Y-axis of the gantry) for a focused image of the root tip. Unlike the search of the root tip (described in section 4.2.1), where the search is performed in image space (along the X-Z plane of the gantry), here the search is performed in the space of the focus measure. Instead of using the entire image, a rectangular region around the image patch with the highest rootness measure is used. The process involves determining the value of the focus measures at a few different positions (along the Y-axis) and estimating the position that would provide a maximum focus score. The description of the focus measure and the search technique used are presented below.

4.2.3.0. Focus Measure

From the work in [9, 15, 24, 29, 35] , it is shown that most focus measures try to measure image properties like gray level image gradients, image contrast or frequency content. In essence they are a measure of the extent of the blur in the image. From a review of previous work on image based focusing, the most commonly used focus measures were identified and are listed below. If we have an image I with height H and width W with $I(x, y)$ representing the gray scale value of a pixel in I located at row y and column x, μ is defined as the mean gray level of the image I, we can define the following focus measures as

a. Tenenbaum Measure (Tenengrad) - The image is convolved with a sobel operator and the sum of the square of the gradients in the x and y direction are computed.

$$F_{tenengrad} = \sum_{H} \sum_{W} S_x(x,y)^2 + S_y(x,y)^2 \tag{4.9}$$

where $S_x(x,y)$ and $S_y(x,y)$ are the results of convolving a window around $I(x,y)$ with the Sobel operators in the x and y direction.

b. Variance - Computes the variations in gray levels in the image.

$$F_{variance} = \frac{1}{H \cdot W} \sum_{height} \sum_{width} (I(x,y) - \mu)^2 \tag{4.10}$$

c. Normalized variance - Similar to the variance measure except the value is normalized with μ.

$$F_{normvariance} = \frac{1}{H \cdot W \cdot \mu} \sum_{height} \sum_{width} (I(x,y) - \mu)^2 \tag{4.11}$$

d. FFT Magnitude - FFT based methods use the log magnitude values of the image in frequency space. The strength of the low frequencies and high frequencies are computed.

$$F_{FFT} = \frac{1}{h \cdot w} \sum^{h} \sum^{w} \log\Big(|\Re e\ I(x,y)|\Big) \tag{4.12}$$

Where $I = FFT\big[I\big]$. h and w determine the region in frequency space (cut off frequencies) within which the frequency strengths are averaged.

Focus measures mentioned above, when evaluated on images of roots, performed in a similar fashion. Fig 4.9 shows sample plots of the focus measures, it can be seen

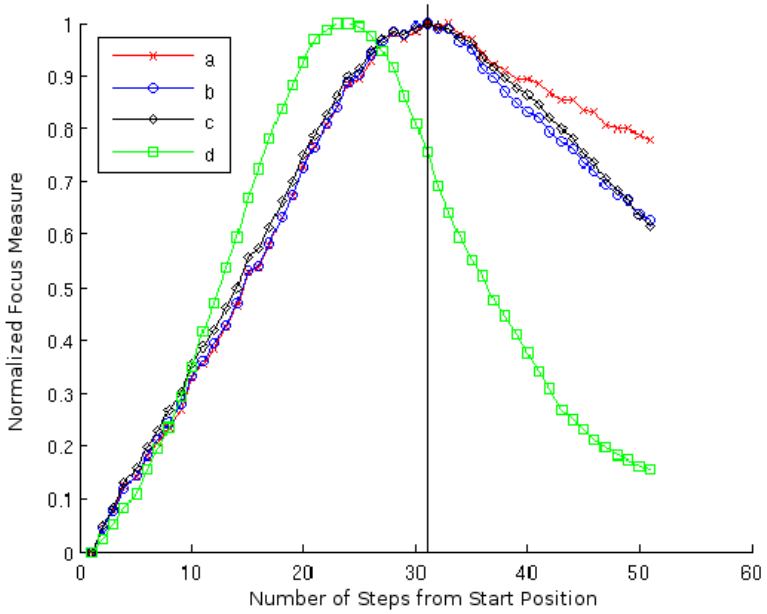

Figure 4.9. Plot showing the four focus measures. a)Tenengrad, b) Normalized Variance, c) Variance, d) FFT Measure. Each measure has been individually scaled to range between 0 and 1. The abscissa shows the number of steps taken from a starting depth at step 0. The ordinate shows the scaled values of the frequency measure.

that the focus measures produce higher values at Y positions that are closer to the best focus position (indicated by the vertical line). The F_{FFT} measure was found to be very consistent but always slightly shifted than the others. On further analysis it was found that this was due to the presence of root hairs which are very small compared to the root and thus contribute heavily to the higher frequency response. This measure is computationally intensive, thus negatively affecting throughput. Owing to ease of computation and simplicity the normalized variance measure was adopted. This focus measure was subsequently used to search for the gantry position with the best focus.

4.2.3.0. Searching Technique for Focusing

Using the focus measures chosen in the previous section a search needs to be performed to determine the location at which the best focused image of the root can

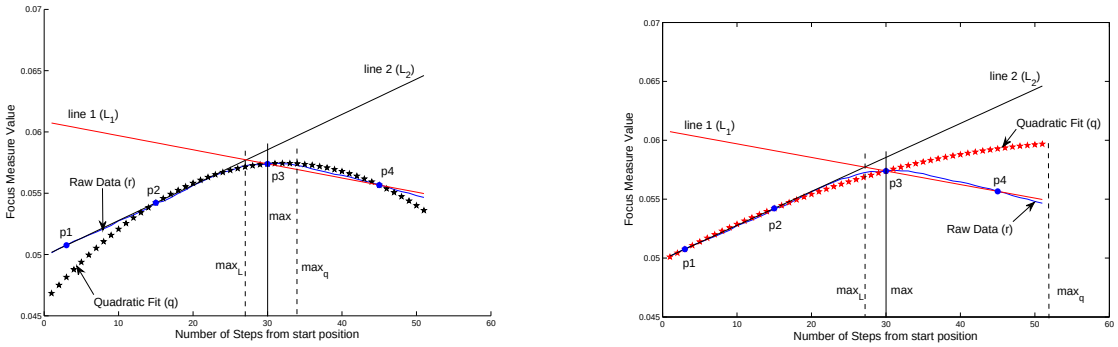

Figure 4.10. Plots comparing two search techniques. The raw data (r), the quadratic fit (q) and the linear fit (L_1 and L_2), when using locations p_1, p_2, p_3 and p_4 are shown. The estimated location of the focus measure maxima is at max_L, max_q and max, for the linear fit, quadratic fit, and manual focusing. The depth of field is about 5 steps and step size is about $50\mu m$.

be obtained. The techniques used to search for the best focused position work under the assumption that the scene contains only one object of interest and, within the search range there exists a single position where the object is in focus (i.e. the focus measure will produce one maxima within the search range). Thus, in theory, the focus measure values can be modeled as a quadratic function and hence the maxima can be determined by obtaining the focus measure at three different gantry positions and the location of the maxima can be directly estimated (shown in Fig 4.10). The estimated location of the maxima is indicated by max_q. This technique of using a quadratic function as a model and determining the maxima has been the most common approach, [9, 15, 24, 29, 35, 14, 28]. From optics literature, given the properties of the lens we can compute the depth of field for varying lens to object distances, using the relation in equation (4.13) obtained from Fig 4.11.

$$\frac{1}{s} + \frac{1}{d} = \frac{1}{f} \tag{4.13}$$

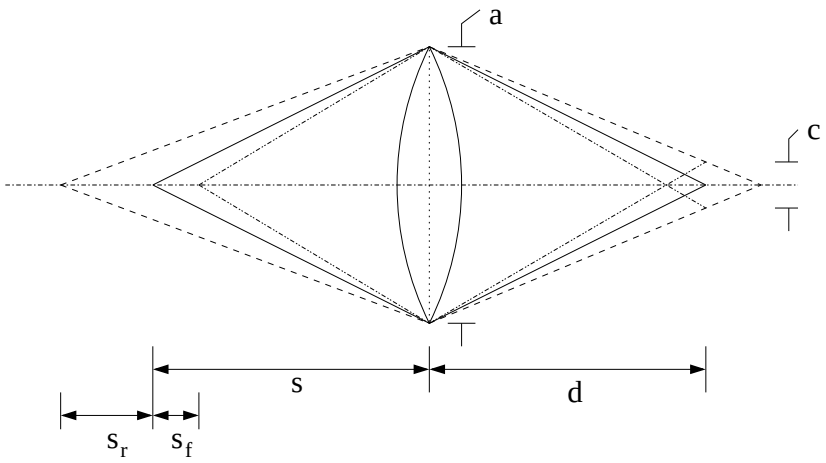

Figure 4.11. Thin lens system with focal length (f), aperture (a), object to lens distance (s), image to lens distance (d), depth of field in front and rear of the object (s_f and s_r).

Where f is the focal length, a is the diameter of the lens, s is the distance of the object from the lens and d is the distance away from the lens at which the image is formed. c is the circle of confusion, it is a value based on the perception of the human eye. The typical value used by photographers is 0.033mm. The value indicates the maximum size of a blurred image of a point object at which the human eye no longer perceives the image as a point (i.e. perceives it as blurred). The values s_f and s_r are distances in front of the object and behind the object up to which the circle of confusion is smaller than c. Using equation (4.13) and the Fig 4.11 we can write the following relations.

$$\frac{1}{s+s_f} + \frac{1}{d\left[1+\frac{c}{a-c}\right]} = \frac{1}{f} \tag{4.14}$$

$$\frac{1}{s+s_r} + \frac{1}{d\left[1-\frac{c}{a+c}\right]} = \frac{1}{f} \tag{4.15}$$

on re-arranging, we have

$$s_f = \frac{sc(s-f)}{fa+c(s-f)} \qquad s_r = \frac{sc(s-f)}{fa-c(s-f)} \tag{4.16}$$

From equation (4.16) it can be seen that the value of s_r will be greater than s_f. This produces an asymmetry, the depth of field in front of the object will be always less than the depth of field behind the object. Thus the values obtained from a focus measure can not be modeled accurately as a simple quadratic curve.

In addition when comparing Fig 4.10(a) and 4.10(b) it can be noted that the curve q changes drastically when the choice of sampled locations change from p_2, p_3, p_4, in Fig 4.10(a) to p_1, p_2, p_3, in Fig 4.10(b) (i.e. the curve changes when the choice of the sampled locations are different, although they may lie on the focus measure curve). This causes the quadratic estimation of the focus measure maxima unstable and sensitive to noise (in the computed focus measure). The quadratic model is not an accurate representation of the occurring phenomenon, where the slopes on either sides of the peak value are different.

From previous work [24, 15, 28], the two most preferred techniques, are a) global Search, b) Fibonacci Search. The global search technique searches the entire depth range with fixed step size to determine the location of the maxima in the focus measure. This is very time consuming and the least preferred option in our case as it will affect throughput significantly. The Fibonacci search has been shown to be optimal, as mentioned in [15], but even this scheme requires at least 10 to 15 images to be captured to determine a stable maximum. The search speed can be increased by using larger step sizes, at the expense of accuracy. In some cases, as discussed in [24, 28], the search is started with a large step size and repeated in a chosen region with smaller step sizes. All of these techniques adversely affect the throughput of our entire system. This is because, if more images are need to determine the focus, more time is spent focusing thus fewer seedlings can be observed in a fixed amount of time.

Based on the discussion in the preceding paragraph we chose to model the focus

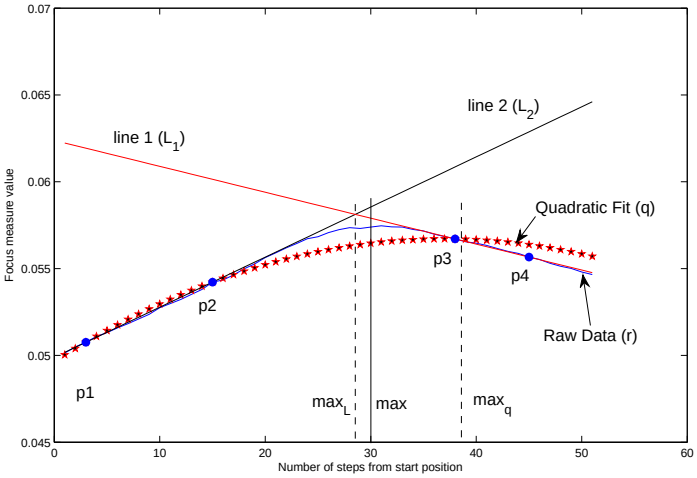

Figure 4.12. Plots comparing the quadratic fit and linear fit. Shows the raw data, the estimate when using a quadratic fit and the line fit. When the sampled locations are changed the linear fit estimate of the peak location is more stable than the quadratic fit estimate.

measure function as two lines whose slopes correspond to the increasing and decreasing trends in the focus measure. This model will better represent the asymmetric nature of the depth of field. We also show (in Fig 4.10 and 4.12) that this model is more resistant to noise in the focus measure and is less sensitive to the sampled positions. The intersection point of the two lines will correspond to the peak value, from which the required position can be estimated. To construct the model, the focus measure needs to be obtained from four images obtained at 4 different locations. The gantry can be moved to these locations and the focus measure is computed from the obtained images. The first two images and the last two images are captured with the small change in the Y position of the gantry. The Y position change between the second and third image is comparatively large. Two straight lines are fit, one to the first two points and another to last two points. The intersection of the two straight lines are computed. This intersection point will estimate the location the gantry needs to move to to obtain a focused image of the root. This process is shown in Fig 4.10. The lines

L_1 and L_2 are fit using the focus measure values obtained from locations p_1, p_2, p_3, p_4. When comparing Fig 4.10(b) and Fig 4.12, it can be seen that unlike the quadratic fit estimate the line fit estimate is more stable when the chosen sample locations are changed (p_3 is shifted) and is less sensitive to noise in the focus measure values.

This method will not guarantee optimal position estimation, as seen by the discrepancy between max_L and max, but will bring the gantry to a location such that the root is located within the depth of field of the lens. The advantage over other search techniques is that it requires far fewer images, hence less time to focus.

Using the above described servoing and focusing technique we have been able to successfully gather image data concurrently for up to 144 seedlings in one session. The following chapter describes the the techniques used to organize and extract features or measurements from the gathered image sequences. The data analysis portion of the workflow is a critical step that will aid in identifying potential phenotypic differences.

Table 4.1. Overall Performance (over 27 gathering sessions) in terms of effective number of seedlings found, i.e., number of useful image stacks of seedlings acquired from which phenotypic information can be extracted. If the system found a seedling and servo to the root tip (bringing it within the field of view) it was deemed a success. The yield obtained for individual gathering sessions is shown in table 6.4.

Seedlings planted (Image Stacks)	3024
Total Failure	633
Number of Seedlings for which useful data could not be acquired due to factors not related to the segmentation technique	289
Good data potentially available	2735
Effective Errors	344
Effective Yield	87.4%

Chapter 5

Data Analysis

This chapter describes the techniques used to extract features from the gathered images of the seedling root tips. The extracted feature information is used to determine if a phenotypic difference exists, when comparing with two or more groups of data. This chapter is broken into two sections. The first section describes how robust features are extracted and the data structures used to organize them. The second half of the chapter discusses how standard machine learning techniques are used with these features to determine if a phenotypic difference exists between different populations of genotypes or between genotypes and a wild type. The machine learning algorithms can be used to identify features of importance through an iterative process. Although the discussion is limited to root tip angle feature in this chapter the described techniques and methodology can be used with other features that can be extracted from the seedling or even the seed.

5.1. Feature Extraction

Feature extraction is the task of reducing the collected images into data relevant to the process of interest so that meaningful information can be inferred. For gravitropic studies the root tip angle data is commonly used for phenotyping. Tip angle curves are the curves (shown in figure 2.5 and 2.7) obtained by plotting the value of the angle between the root tip and the horizontal with respect to time. We chose the tip angle curves over other features as our test bed because it is one of the most commonly used features for phenotyping. In this section we describe the steps involved in feature extraction, figure 5.1 shows the three stage feature extraction process, which we describe below.

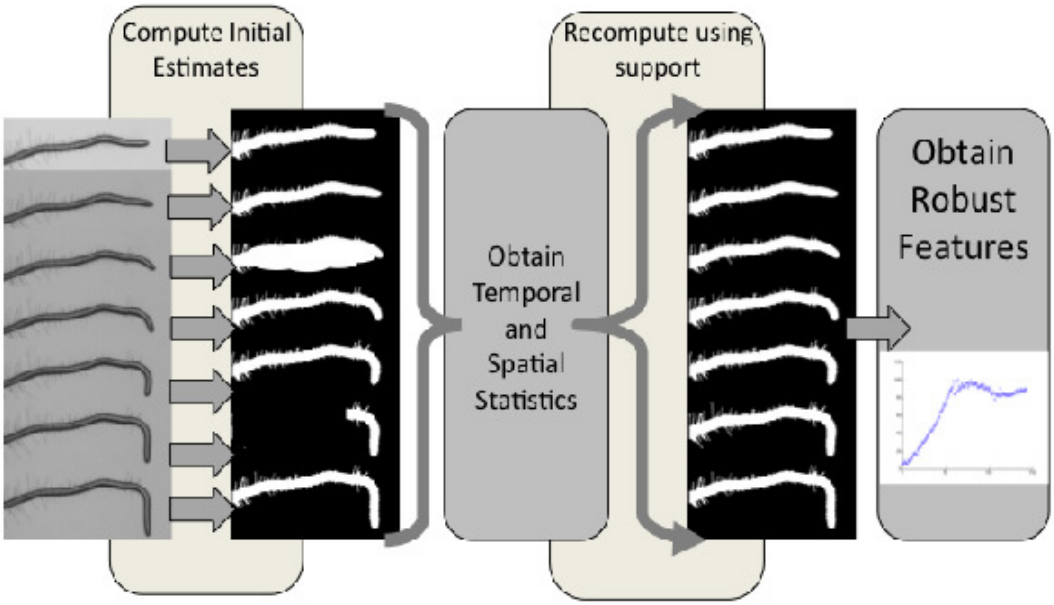

Figure 5.1. Feature Extraction Pipeline

- Stage I: In stage one, the images are organized as a time lapse sequence or a stack. Each image in the stack is initially processed independently using the root segmentation technique described in section 4.2.1.

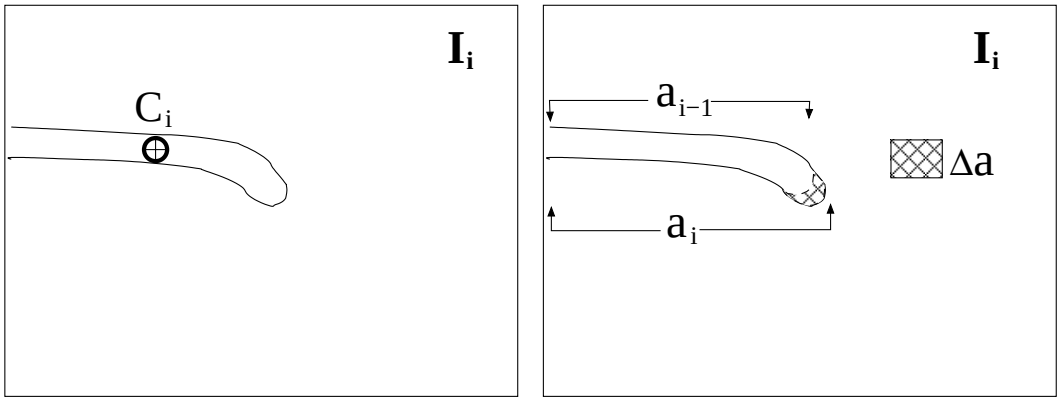

Figure 5.2. Images showing C_i and Δa_i

- Stage II: Here the performance of the segmentation process is evaluated by computing statistical measures from the stack of independently segmented root images. The measures used are (i) location of centroid of the root in the image at each time point, and (ii) change in area (size) of the root (with respect to the previous time point in the stack). The mean and standard deviation of these measures are computed as discussed below and shown in figure 5.2. Given a stack with t time points the i^{th} binarized image I_i has a root with an area a_i and the centroid of the root patch is C_i. Where $C_i = (x_0, y_0)$ represents the location of the centroid at location x_0, y_0 in the image I_i. The area change is given by

$$\Delta a_i \;=\; a_i - a_{i-1} \tag{5.1}$$

The mean and standard deviations for the centroid and area change measure are

$$\bar{C} \;=\; \frac{\sum_{i=1}^{t} C_i}{n} \tag{5.2}$$

$$\Delta\bar{a} \;=\; \frac{\sum_{i=2}^{t} \Delta a_i}{n-1} \tag{5.3}$$

Using the computed mean and standard deviation values $\bar{C}$, σ_C, $\Delta\bar{a}$ and $\sigma_{\Delta a}$, images are checked for outliers and the outliers are flagged for correction. Images

with values two standard deviations or more away from the mean are flagged for correction. Additionally, the image with C_i and Δa_i value closest to $\bar{C}$ and $\Delta\bar{a}$, respectively, is chosen as the model image, I_m.

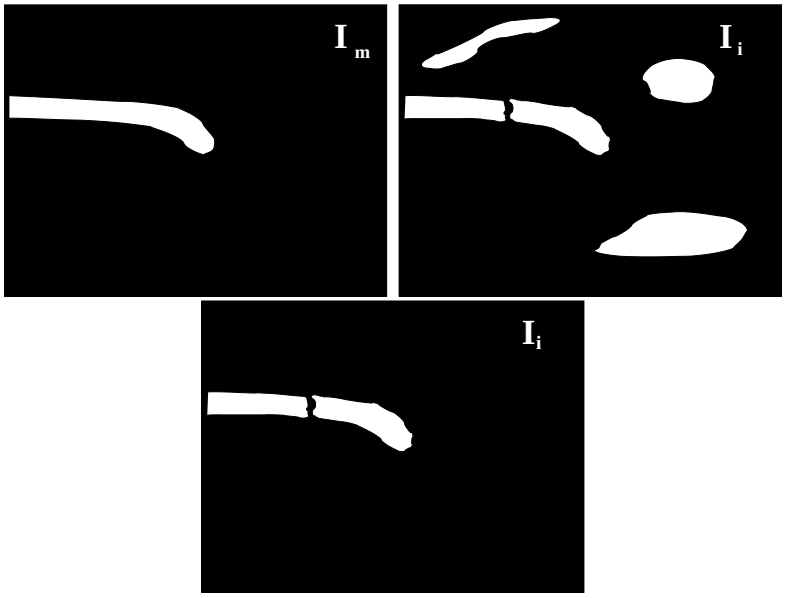

Figure 5.3. Images showing $\tilde{a_i}$ and I_m are used to identify the root when a discontinuity is present. $\tilde{a_i}$ is used as a size estimate to determine if the chosen set of patches closely matches the estimated size. The model image I_m (left) is used to identify candidate patches that may need to be included to represent the entire root. This helps overcome small occlusions. The occlusions cause a break in the root patch (right). The gaps can then be filled in to make a single root patch.

- Stage III : The images flagged in stage two are reanalyzed incorporating $\bar{C}$, $\Delta\bar{a}$ and I_m. This is done by using I_m as a template to identify all potential root regions in a given image. $\bar{C}$ is used to modify equation 4.7. $\Delta\bar{a}$ along with a_{i-1} is used to estimate the area of the root in the flagged image. The value of p_{root} in equation 4.7 is adjusted by adding an extra weighting factor w_4^j, where j is the j^{th} patch in the image I_i.

$$p_{root}^j = w_1^j \cdot w_2^j \cdot w_3^j \cdot w_4^j \cdot p_{avg}^j \tag{5.4}$$

$$w_4^j = 1 - \frac{D_j}{D_{max}} \tag{5.5}$$

where p_{avg}^j is as defined in section 4.2.1. D_j is the euclidean distance of the centroid of the j^{th} patch from $\bar{C}$ (the computed mean centroid location). D_{max} is the maximum distance between $\bar{C}$ and the end of the image (this usually is the distance to one of the corners of the image).

The model image I_m, $a_i - 1$ and $\Delta\bar{a}_i$ are used if the chosen patch does not meet the area requirement as discussed in stage two. This would imply that only a part of the root has been found (see figure 5.3). This would be the case if the root, in the image, was partially occluded due to a scratch, condensation droplet, air bubble, etc. I_m is used as a template to identify all the patches in I_i that share pixels with it. We call this subset of patches in I_i as B_i. The patches in B are ordered by their rootness value. The area of the root in the flagged image is estimated as

$$\tilde{a}_i = a_{i-1} + \bar{\Delta a} \tag{5.6}$$

To obtain a binarized root image with the required size and location, patches from B are added (int descending order of p_{avg}) to the image until the size and position requirements are met.

The three stage process described above will help identify and fix outliers. Once the segmented images are obtained they need to be reduced to a set of usable features. The discussion of the feature extraction here is limited to the extraction of tip angles. It also intuitively extends to extraction of other features from the entire seedling. Other features that can be extracted from the root images are curvature along the root, growth rate, etc.

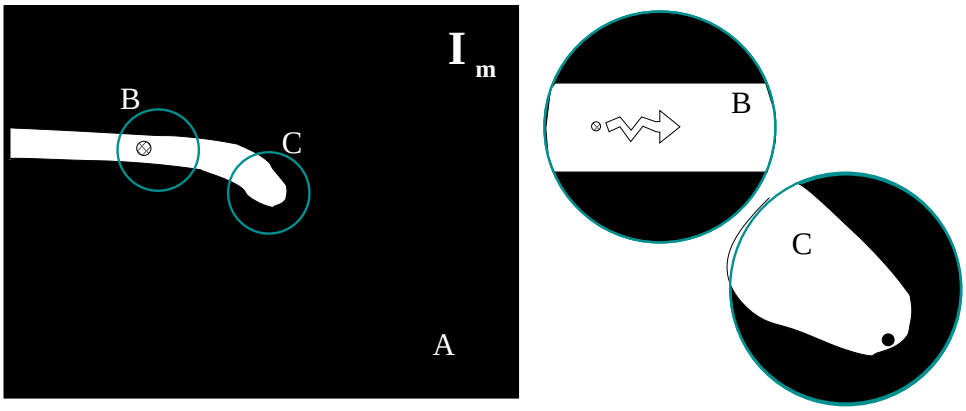

Figure 5.4. Monte Carlo based root tip finding. A: Initialize points starting near C_i. B: Allow the particles to "flow" through the root. C: Identify stopping point as possible root tip location (close to the root tip).

To extract the root tip angle information the binary images are reduced to their skeletal representations using the technique described in [36]. The root skeleton is stored as a graph (as shown in figure 5.5). The graph representation allows for non trivial root systems to be stored while preserving the structural representation. The same representation can be adopted to represent the entire seedling. Once the root (or seedling) is converted into the graph representation, features like root tip location, root tip angle, curvature at all points, tip angle or branch angle of non trivial root systems can be readily computed. The steps involved in obtaining the graph representation are (1) Tip identification, (2) Skeletonization and pruning, and, (3) Graph representations. The tip identification step is required to identify all possible root tip locations. These tip locations will help prune the skeletonized roots and serve as a starting point to develop the graph based representation, and is described below.

Root tip localization algorithm :

1. The process starts by determining a set of starting points on the root. The point on the root closest to the centroid is chosen. The chosen points are akin to particles and they are allowed to "flow" (as shown in figure 5.4 similar to a

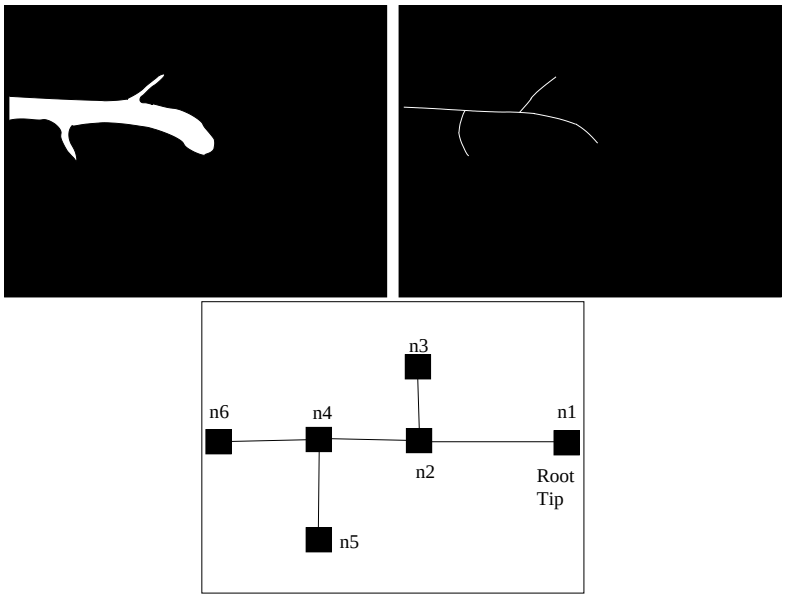

Figure 5.5. Images showing a binarized root and its corresponding graph representation.

Monte Carlo (MC) experiment. The image points at which many particles settle are all marked as candidates for tips. For complex root systems the root tips are the location that have been identified by both the particle flow and have a skeletal end point near them. For the current application the seedlings only have their primary roots present (i.e. they only have 1 root tip). Thus the root tip is identified as the location where most particles settle.

2. In the next step the binarized root is reduced to its skeleton using standard approaches [36, 16]. The spurious end and branch points are removed if the the tip of the branch does not end near, or lead to, any of the chosen end points from step 1. This pruning step helps remove spurious branches and removes branches that may be caused by root hairs, etc.

3. The skeleton that is obtained after the pruning step is mapped to its representative graph. The nodes in this graph represent branch and end points. The graph edges are the skeletal pixels connecting the nodes, shown in figure 5.5.

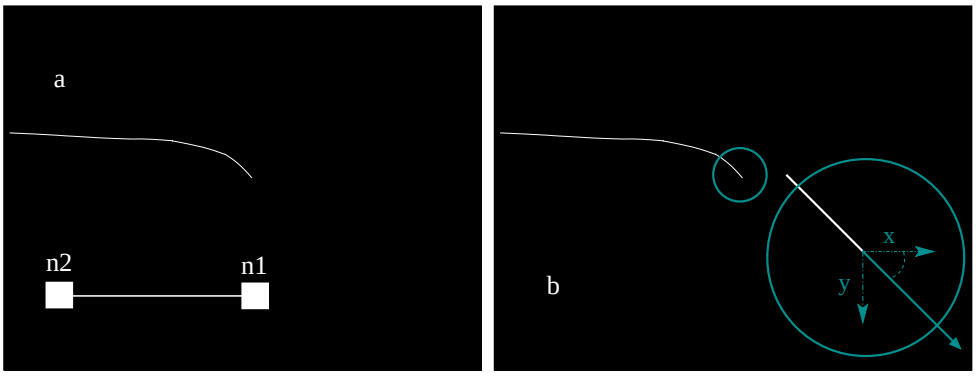

Figure 5.6. This figure depicts the steps involved in extracting the tip angle from the binary images using splines.(a) Raw skeleton of the root after pruning. $n1$ and $n2$ are nodes of the graph representing the root. (b) The spline fit to the root data computed from the graph. The angle computed at the end of the skeleton estimates the angle of the root tip.

This technique can be used to represent non trivial root systems and can be used to represent the leaves, cotyledons and hypocotyls as well. This representation preserves the general structure of the seedling and provides a structure for storing all the feature data.

Once the graph representation is available many features can be computed and stored in the graph data structure. For the current application the root tip angle is computed by fitting a spline to the edge connected to root tip node. The angle at the end node of the spline is used as the tip angle. When the tip angle values are extracted for the entire stack we have a tip angle plot that shows a roots response to a change in gravity stimulus. Figure 5.7 shows a sample plot.

The time course change in tip angle features is a representation of the root tip's response to the change in gravity stimulus. A sample plot of the change root tip angle over time is shown in figure 5.7 These tip angle curves (figure 5.7) are used as the features to detect phenotypic differences between different genotypes. The technique to find phenotypic differences are discussed in the following section.

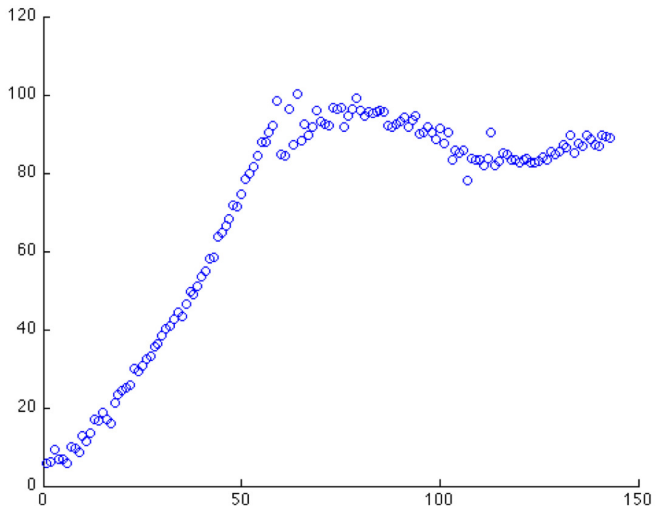

Figure 5.7. Sample tip angle plot obtained from the tip angles calculated from one stack of images, corresponding to the gravitropic response of one seedling.

5.2. Data Interpretation

Data interpretation step involves using extracted features from the images (e.g. root tip angle values extracted over all time points, for a particular seedling) and performing a preliminary analysis automatically. The preliminary analysis helps identify features of interest. In the context of root tip angle curves, time points of interest, where different genotypes behave differently, can be identified. This will reduce the complexity of successive analysis, e.g Quantitative trait locus (QTL). The analysis described in this chapter involves using standard machine learning algorithms to determine if two or more genotypes display any phenotypic differences.

The machine learning (ML) algorithms are used together as an ensemble of supervised classifiers. The ML algorithms that have been used are Naive Bayes, Random Forests, Bayes Nets and Multi Layer Perceptrons [20]. These algorithms are available as Java libraries from the software package WEKA [10]. Classification can be

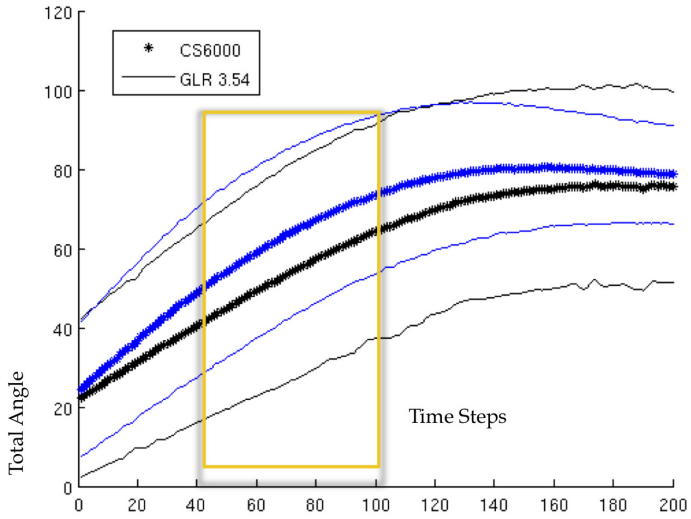

Figure 5.8. Plot showing showing a phenotypic difference between one genotype and its corresponding wild type (or control gene).

performed on the data in different ways based on the representation of the data. We describe two such representations. (1) Treating each tip angle value at each time point as feature, thus the tip angle values from a stack would form one single feature vector, (2) Treating each feature independently to determine if a phenotypic difference occurs at a particular time point. An example of tip angle data having phenotypic difference is shown in figure 5.8. The genotype in this figure was identified as being phenotypically different from its corresponding wild type using representation type (1). While representation type (2) was used to determine the time points where the phenotypic difference exists.

An alternate analysis can be performed on the tip angle data such that the inferences obtained from representations (1) and (2) can be obtained simultaneously. This is made possible by choosing a representation that describes the tip angle curve rather than using all the tip angle values. One technique is to fit the data to a representative parametric form and use the parametric equation for comparisons. In current

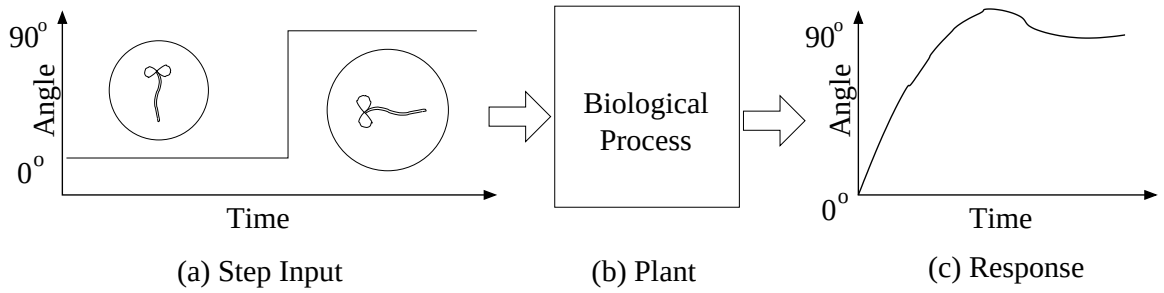

Figure 5.9. The seedling responding to a change in gravitropic stimulus can be considered as a second order system with a step input. The tip angle plot is the system response to the step input.

scenario we use a representation taken from linear system and control theory. The tip angle curve is represented by a set of descriptive features that are typically used to describe system response curves, e.g. time constant, peak time, rise time, area under the curve, peak value and final value. Thus treating the gravitropic mechanism as a linear system. The advantage of this representation is that it simultaneously combines information from (1) and (2), in addition, it reduces the size of the feature set from about 140 to 200 features to about 10. Figure 5.10 shows the tip angle curve with the above mentioned features appropriately labeled.

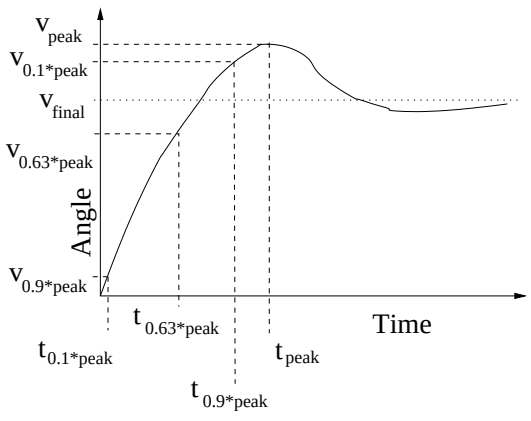

τ	Time Constant. $t_{0.63*peak}$
t_{peak}	Peak Time.
$t_{0.1*peak}$	Time at 10% Peak Value.
$t_{0.9*peak}$	Time at 90% Peak Value.
t_{rise}	Rise Time. $t_{0.9*peak} - t_{0.1*peak}$
auc	Area Under the Curve.
V_{peak}	Peak angle value.
$V_{0.9*peak}$	90% Peak Value
$V_{0.1*peak}$	10% Peak Value
V_{final}	Final angle value.

Figure 5.10. This plot shows the features used to represent the tip angle curve. The terms are described in table on the left.

When dense feature sets are made available to represent a process, performing

detailed analysis on such data with large dimensions (e.g. 300 dimensions) can be a tedious, time consuming and complex. This burden can be reduced by removing features of little value to the feature analysis process (e.g QTL). Here we propose a two step process for identifying features that are good candidates for phenotype analysis, when comparing two or more populations of genotypes. Stated differently, if two (or more) populations of genotypes are considered this technique identifies the features that most accurately classifies the data into two (or more) groups. The process uses multiple machine learning classifiers such that each classifier identifies a feature subset. The feature subset that performs on average the best (when used with all the classifiers) is picked as the most representative subset.

If we have a set of features $\mathbf{f} = \mathbf{f_1}, \mathbf{f_2}, \ldots \mathbf{f_n}$ and a set set of classifier $\mathbf{C} = \mathbf{C_1}, \mathbf{C_2}, \ldots \mathbf{C_m}$ where $n >> m$.

- Step 1 : $\forall C_i$ in $\mathbf{C}$ we can identify a set of features $\mathbf{f_{C_i}} \subseteq \mathbf{f}$. Each $\mathbf{f_{C_i}}$ is a candidate for the best representative subset for the data. The subset is identified using standard implementation using the WEKA library, with a greedy search technique and a threshold of 95% accuracy.

- Step 2 : Each $\mathbf{f_{C_i}}$ is then used with set of classifiers $\mathbf{C}$ and the set that produces the highest average accuracy value is chosen as the best feature subset.

The ML based phenotyping technique has the advantage that it can be readily extended to analyze a complex collection of features, e.g. seed morphology features, chemical composition, shoot and hypocotyl morphometric features. In addition, this technique can be used to identify or reduce a given feature set by removing features that have low discrimination (phenotypically) power.

The techniques described in this chapter form the post processing stage of the

workflow. This stage performs the critical task of feature extraction, reduction and selection. The selected features allow the plant biologist to focus on a subset of the data reducing the effort and time required for further detailed studies. Having described all the parts of the workflow it is required to test and evaluate the workflow to identify problems, improve throughput and to determine the variations in measured features due to the variation in acquired images and the image processing techniques. The following chapter describes in detail the performance analysis of the automated workflow and the design changes that have been incorporated to improve the system.

Chapter 6

System Performance Evaluation and Results

In this chapter we evaluate the performance of the system, enumerate situations where the system fails (does not acquire useful data) and categorize reasons for such failures. We provide an analysis of the throughput, identify system bottlenecks and provide a discussion of the data analysis. The collected data from each seedling is deemed "useful" or "good" if roots can be identified and measurements can be reliably extracted. Thus our criteria for assessing performance is measured with respect to the useful data gathered. In this chapter the following sections first analyze the system as a whole, followed by a discussion of the acquisition and the data analysis components of the pipeline.

6.1. Cost Analysis

In addition to analyzing the way the system operates and performs, we carried out an analysis of the cost to setup the system and how these costs would change

Table 6.1. Robotic System *vs* other Semi-Automated Systems

System Type	Seedlings observed	Spatial Resolution	Approx. setup cost / seedling
Manual (1 camera, 1 seedling)	Very low (one)	High	High
Semi-Automated (1 camera, many seedlings)	Many (10 to 20)	Low	Low
Semi-Automated (10 cameras, 10 seedlings)	one per camera	High	High
Robotic	Very High (current max. 324)	High	Low

as the acquisition system scaled. The costs are representative and were only used to determine if the setup cost would be high or low in each case. Table 6.1 qualitatively shows the cost per seedling for the entire imaging equipment along with some of the pros and cons of each type.

The single camera system referred to here is similar to those used in [19]. Table 6.1 gives an approximate (order of magnitude) setup comparison for the high throughput options. When scaling the size of the study the robotic system has a much lower amortized setup cost.

The average cost of capturing data for one seedling is about $4000.00 US while the robotic visual servo system currently under investigation amortizes the cost to about $600.00 US per seedling (potentially as low as $250 with more seedlings per Petri dish). These costs are costs to set up the first data gathering session. Due to the higher throughput of the robotic system the costs will amortize to much smaller values very quickly when compared to other data acquisition methods.

6.2. Design Analysis and Bottleneck Identification

6.2.1. Timing Analysis and Gathering Capacity

Temporal sampling is the shortest time between two observations of a feature of interest on a seedling. Typically, this can range from a few hours to about $5min$ depending on the nature of the phenotype. In the case of a manual data gathering process a few (typically 5 to 10) seedlings are imaged every hour or two. With the semi automated scenario one camera focused on one seedling can gather image data of the region of interest at a resolution of about $2min$ or less. With the robotic system at present, with the cassette loaded with 144 seedlings, the resolution is about $7min$ (with the exception of the time gap between the first time point and the second time point, discussed later in this section).

To clearly understand the temporal resolution of the robotic system we outline the steps involved in data acquisition process. The data gathering is broken down into two stages. Stage 1, is the determination of the locations of the root tips for all the seedlings. The gantry visually servos to the tip of the root and records the locations. Stage 2 involves repeated visits to the recorded locations to capture the changes occurring at the root tip. Stage 1 is performed once per data gathering

session and is time consuming, currently requires about 17 to 20 min to complete. Stage 2 consists of multiple passes over the cassette to the recorded locations, with each pass taking 3.5 min (these stages are shown in (6.5)). The major factors that affect the temporal resolution are

(a) Size and speed of system.

(b) Complexity involved in identifying region of interest.

(c) Number of seedlings

The following equations provide a detailed break down of the time, for which the data gathering is performed. This will help discuss and better understand the performance and bottlenecks of the system.

$$t_{gath} = t_{pos} + t_{settle} + t_{cap} \tag{6.1}$$

$$t_{gatherall} = N * t_{gath} \tag{6.2}$$

$$t_{loc} = t_{focus} + t_{find} + t_{servo} \tag{6.3}$$

$$t_{fp} = t_{loc} * N \tag{6.4}$$

$$t_{tot} = t_{fp} + n * t_{gatherall} \tag{6.5}$$

Some of the variables mentioned above have a very small impact on the throughput of the system or have a time period that is fixed, e.g. t_{pos} depends on size and speed of the system and is fixed by design. The gantry robot with its high speed, large size and high accuracy, allows all motions to be less than 1 second, thus keeping t_{settle} to be about 1 second. Considering the speed of camera and computer, t_{cap} and t_{find} each are much less than 1 second, thus are not very critical for the the analysis of

N	Number of Seedlings.	t_{tot}	Total time for data acquisition.
n	Number of time steps to be captured.	t_{loc}	Time to locate seedling.
t_{pos}	Time to move robot to a given position.	t_{fp}	Time to locate all seedlings on the first pass
t_{find}	Time to segment the root.	t_{gath}	Time to gather one image from one location.
t_{settle}	Settling time provided to prevent motion vibration from causing image blur.	$t_{gatherall}$	Time to gather one image from all location in the cassette.
t_{servo}	Time to servo to region of interest (root tip)	t_{onset}	Estimate of the time lapsed between the change in stimulus and the seedlings first response
t_{focus}	Time to determine proper focus.		
t_{cap}	Time to capture and store image data of region of interest.	$t_{complete}$	Estimate of the time lapsed between the change in stimulus and the seedling reaches a steady state

the system performance. In this section the performance (throughput) of the system is analyzed from two different view points, (i) the user (plant biologists) and (ii) the system design. From the user perspective (plant biologists), who define the biology that needs to be observed (in this case the response of the root to change in gravity field) and the length of the data gathering session, there are two primary concerns

(a) Timing - Amount of time required to locate and image all the seedlings in the Petri dish cassette.

(b) Yield - Number of Useful seedling data gathered per session.

The system is designed such that during the first pass over the cassette, time is spent locating and focusing on each seedling (equation (6.4)) (in addition to the time spent collecting the image data, equation (6.2)), as described above. This makes the first pass through the cassette longer than each of the other passes. For the subsequent passes the system requires a shorter, albeit finite, period of time. These two parameters

t_{fp} and $t_{gatherall}$ implicitly effect the system performance for the user.

Equation (6.4) computes the amount time taken for the first pass, this specifies the lower limit of the biological process that can be observed.

From equation 6.2, we can determine the total amount of time required to gather data for one full pass over the cassette. This will determine upper limit of the speed of the biological process. Any biological process that has an onset time (t_{onset}) greater than t_{fp}, but a completion time ($t_{complete}$) smaller than $t_{gatherall}$ will be under sampled. Thus N, will have to be scaled based on the speed of the biological process. Currently, even with 72 seedlings planted in the cassette, $t_{gatherall}$ is approximately 3.5 min (the time gap between two successive images of a given seedling). This time resolution is much faster than a typical biological process, which are in terms of hours. Hence is not of critical concern to the throughput. This can be seen from the following equation.

For determining the number of seedlings, N, that can be observed in a session, we have the following constraints from the above discussion

$$t_{fp} < t_{onset} \qquad t_{gatherall} < t_{complete} \tag{6.6}$$

$$N < \frac{t_{onset}}{t_{loc}} \qquad N < \frac{t_{complete}}{t_{gath}} \tag{6.7}$$

Using equations (6.4) and (6.2) and rearranging we have equations (6.7). As mentioned above, $t_{complete} \gg t_{gath}$, thus the value of N is determined by equation (6.8), but for a generic gathering session we would pick the lower N value.

$$N < \frac{t_{onset}}{t_{loc}} \tag{6.8}$$

We can compute N for a typical data gathering session. If we have $t_{loc} = 15$ sec and set $t_{onset} = 20$ min, we have $N = 80$ seedlings. Thus we chose to use $N = 72$ (2

seedlings per plate and a total of 36 plate in the cassette). The value of t_{onset} can also be viewed as the as the maximum time that the biologist is willing wait before regular observations of the seedlings will be available.

With the current PDCU design all seedlings are rotated simultaneously, i.e. all the seedlings are provided with a gravitropic stimulus at one instant. Hence the first image data captured for each seedling is obtained at different times after the time of stimulus. This may seem to make t_{fp} a bottleneck. But this is not the case. If an alternate technique was used such that the seedlings are turned individually just prior to being imaged for the first time rather than all together, each seedling will be imaged immediately after being subjected to a gravitropic stimulus. It will seem like t_{fp} is no longer a bottleneck as t_{fp} will be small for each seedling. But even in this case a bottleneck will arise, as the second pass must start before t_{onset}. There is no advantage as the total amount of time required to go through the cassette (t_{fp}) will be the same, as determined by t_{onset}. In addition the design of the PDCU will become more complicated as it will have to include a mechanism to turn each Petri dish independent of the other dishes.

6.2.2. Metrics

The metrics for throughput and performance are broadly classified into two categories from the view points of design and usage. The first category is from the view point of plant biologists, which provides information about the throughput with respect to the seedlings. The second category provides the performance details for visual servoing. Although all the listed metrics are implicitly related, each one of them will highlight the performance of different aspects of the automated plant phenotyping system. A seedling is deemed *usable* if the images collected by the system can be

subsequently used for phenotype data extraction, otherwise the seedling is termed a *failure*.

6.2.3. Category I - Biologically Relevant

The following two metrics will help observe the throughput of the system in terms of the number of seedlings and with respect to the temporal resolution between two images of the same seedling

Seedlings Per Session (SPS) - The SPS is determined using the number of *usable* seedlings during a particular data collection session. The cases where the system failed due to the image processing are considered. Failures due to non-systemic reasons (e.g. missing seedling, etc) are also taken into account. Thus the number of useful seedling will also indicate the effective yield for a given session.

$$|\mathbf{Useful\ Seedlings}| = |\mathbf{Seedlings}| - |\mathbf{Seedlings\,Lost}|$$

$$\mathbf{Seedlings\,Lost} = \{\mathbf{Seedlings}|\mathbf{SystemErrors}\} \bigcup \{\mathbf{Seedlings}|\mathbf{NonSystemErrors}\}$$

$$\mathbf{IPS} = \frac{|\mathbf{Useful\ Seedlings}|}{\mathbf{session}} \tag{6.9}$$

Total Localization Delay per seedling (TLD) - The TLD time is the amount of time required for the system to determine the location of each seedling and visually servo to the required region on the seedling (described in the TTT metric), the region of interest is the root tip of the seedling, summed over the whole grid. As this process is carried out only once at the start of data gathering

session, the delay only occurs once and does not effect the subsequent data gathering. Ideally, the TLD should be as close as or less than the TR metric, discussed below. This time delay is unavoidable and will quickly add up as the number of seedlings increase.

$$\mathbf{TLD} = \sum_{\mathbf{PDCU,time=0}} (\mathbf{Time\,to\,Locate\,Seedlings} + \mathbf{TTT}) \tag{6.10}$$

Time Resolution (TR) - The time resolution is the time period between two successive images of one seedling, in the PDCU, captured and saved during a session. This time resolution is dependent on the design specification and the actual time the system requires to visit every seedling in the PDCU and the number of seedlings present in the PDCU. The time between two samples of the same seedling is calculated independent of the TLD. The time resolution will be directly effected by the number of seedlings present in a Petri dish.

6.2.4. Category II - Relevant to System Performance

The metrics listed below will provide a basis for analyzing the throughput and performance of the robotic system.

Seedling Data Per Unit Time (SDPU) - The data acquisition can be expressed in two modes. First, in terms of the number of seedling images acquired per minute (averaged over the entire data gathering session). Secondly, in terms of the number of bytes of data acquired per minute. Both metrics will provide information about the data throughput either in terms of the seedlings or in terms camera resolution. this metric gives details of the amount of useful image information saved (this will account for any intermediate data that will be saved,

either to aid phenotype extraction or measure system performance).

$$\textbf{SDPU} = \frac{\textbf{\# Bytes of Seedling Data}}{\textbf{minute}} \tag{6.11}$$

When the SDPU is computed separately for the first pass it will provide information about the time required to localize the root tip. While the metric when computed for all other passes will provide information about the effect of the settling time (required to avoid motion blur effects) on the throughput.

Images Analyzed Per Saved image (iAPS) - This metric will provide an estimate of the efficiency of the analysis technique. The fewer the number of images that need to be analyzed to obtain each *usable* image the better. Considering that all the analysis for localizing and servoing are performed during the first pass through the PDCU, this metric is computed only during the first pass.

$$\textbf{iAPS} = \frac{\textbf{\# images analyzed}}{\textit{usable image saved}} \tag{6.12}$$

Time To Target (TTT) - The time required to locate a root tip after the seedling has been localized, averaged over all seedlings in the PDCU, is the TTT. All planted seedlings are taken in to account. *Failed* seedlings are considered and the corresponding TTT is computed separately.

Target Centeredness Distribution (TCD) - The recorded location of the root tips for each seedling in the PDCU are used to generate a distribution indicated by the deviation from the ideal location. Ideally the result of the visual servoing should bring the root tip to the center of the field of view. But the deviations can be caused due to positioning accuracy and resolution of the robotic system and the control technique used. There can be errors introduced due to the image processing algorithms used.

Good Focus Metric (GFM) - Metric for grading the quality of focus of the roots in a given image will effect the results of the image processing techniques used to localize and servo. Currently very basic metric is used by measuring the average mid-frequency content in the frequency space of a given image.

The measures discussed above will be useful in determining parameters that may affect the system. The parameters listed below not only effectively describe the performance or throughput, but also form a major part of the design specifications. This will help link the overall performance of the system with the initial design parameters, discussed earlier in section 3.1.2 :

- Robot Position Resolution
- Robot Position Error
- Camera Resolution
- Number of seedlings per Petri dish
- Focus
- Single (vs) Two-Stage

The results of the analysis with the system and the measurable properties have been summed up in the two tables 6.2 and 6.3. The tables clearly highlight two system parameters critical for system performance: focus and visual servo design. The initial visual servo loop was modified to incorporate the two step servoing (servoing with low magnification camera first and then servoing with the high magnification camera for higher precision). The techniques used for focusing were updated to produce better throughput performance.

Table 6.2. Measurable Properties and their effect on the parameters of interest.

Measurable Properties	Seedlings Per Session (SPS)	Total Local--ization Delay (TLD)	Time Res (TR)	Seedling Data Per Unit Time (SDPU)	Images Analyzed Per Saved image (IAPS)	Time To Target (TTT)	Target Centere--dness Distrib. (TCD)
Seedling Size	√			√		√	
Number of Seedlings	√			√		√	
Focus	√	√	√	√	√	√	√

6.2.5. System Bottlenecks

The gantry robot with accuracy shown in table 3.1 and a calibrated camera with a resolution of $5.5\mu m/pix$ allow for very high servoing accuracy. A simple visual servoing loop is used as discussed in [5, 6, 11], with a scaled orthographic model for the camera and simple translations for all motion. In addition, the desired accuracy is set so that the servo is deemed complete when the root tip is within a $100pix$ of the center of the field of view. This ensures that t_{settle} remains small and thus the robotic system does not bottleneck the throughput.

From the analysis of the system in the earlier part of this section we can identify the most critical parameters of the system that can effect the throughput. The bottleneck can be identified by analyzing the temporal sampling ability. This is the shortest time between two observations of a seedling. This is determined by the term $t_{gatherall}$

Table 6.3. Measurable Properties and their effect on the parameters of interest Contd..

Measurable Properties	Seedlings Per Session (SPS)	Total Local--ization Delay (TLD)	Time Res (TR)	Seedling Data Per Unit Time (SDPU)	Images Analyzed Per Saved image (IAPS)	Time To Target (TTT)	Target Centere--dness Distrib. (TCD)
Robot Pos Resolution						√	√
Position Error						√	√
Camera Resolution						√	√
Single Step Servoing	√	√	√	√	√	√	√

given by equation (6.2). Typically, this can range from a few hours to about 5 min depending on the nature of the phenotype. In the case of a manual data gathering process a few (typically 5 to 10) seedlings are imaged every hour or two. With the semi automated scenario one camera focused on one seedling can gather image data of the region of interest at a resolution of about 2 min or less. With the robotic system at present, with the cassette loaded with 72 seedlings, the finest resolution is about 3.5 min (with the exception of t_{fp}, first pass time which is about 17 min). The major factors that affect the temporal resolution are (a) Size and speed of system and (b) Number of seedlings.

From equation (6.2) it can be seen that t_{gath} increases linearly with increase in N,

number of seedlings. Also, owing to the accuracy and speed of the system all values in t_{gath} are small, which when improved will lead to a total reduction of $t_{gatherall}$ by 5%. Thus, this is not a critical bottleneck.

In the case of t_{fp}, as discussed in section 6.2.1, t_{servo} and t_{focus} constitutes the largest share of the time. Using equations (6.4) through (6.5) it can be seen that maximum gain in t_{fp} can be obtained by reducing t_{servo} and t_{focus}. This will allow for an increase in throughput when collecting data for biological processes with earlier onset times (t_{onset}, discussed in section 6.2.1). t_{servo}, time taken to servo to the root tip, is dependent on the length of the seedling and varies between 1 and 5 seconds, while t_{focus}, time to focus on a given root is typically between 5 and 16 seconds. Thus reducing focusing time by 5 seconds can reduce t_{fp} by about 25%. Thus establishing that the critical bottleneck for t_{fp} is currently the focusing process and further research is required to provide faster on-line focusing technique.

6.3. Data Acquisition Performance

6.3.1. Data Losses due to external factors

Some of the situations where failure to collect data is due to factors not related to the robotic platform are itemized below with examples shown in the figures.

(a) Scratch on agar medium - A scratch in the agar imaged in infra red light contains many features similar to a young seedling (about 2 days old). These are erroneously marked as seedlings (see figure 6.1(i)).

(b) Peeling of the agar medium - In some cases the agar peels away from the plate and thus produces a long root like artifact, which the servoing system erroneously identifies as a root (see figure 6.1(ii)).

Figure 6.1. (i) Scratches (ii) Peeling of agar.

Figure 6.2. (i) Growth out of focus plane (ii) Non germinating seed.

(c) Root growth out of the depth of field - This phenomenon occurs in two forms, both causing focusing problems. The first, the root during the first day or two of the germination process has grown into the agar medium rendering one part of the root at one depth and the other at another (figure 6.2(i)). The second case, occurs when the root grows into the agar during data collection. Both cause the data gathered to be out of focus and almost impossible to use.

(d) Non or late germination - Some seedlings do not germinate or germinate much later than majority of the other seedlings (see figure 6.2(ii)).

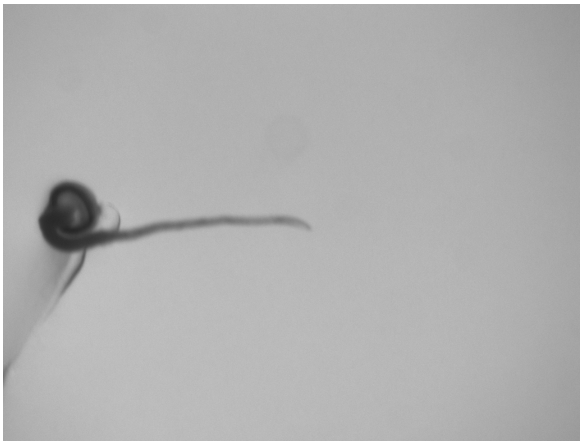

Figure 6.3. Seedling with thin roots.

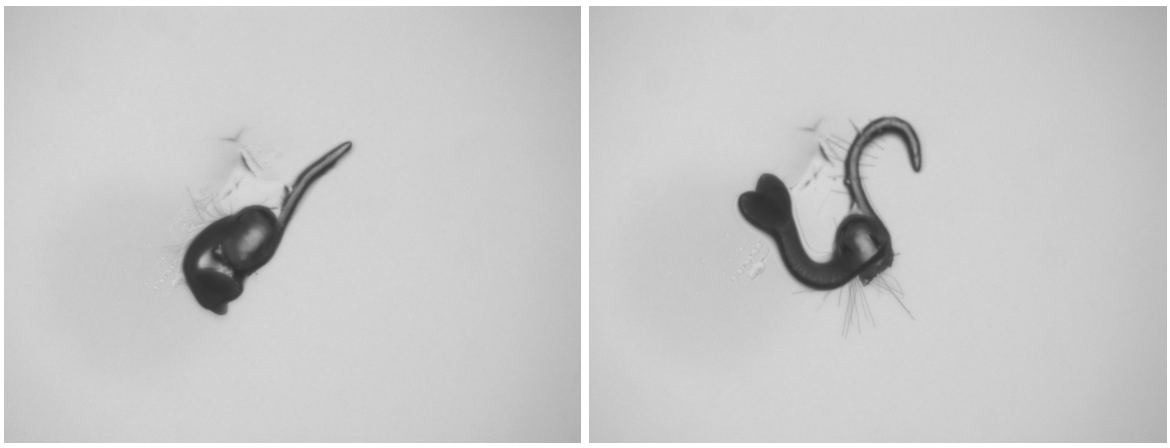

Figure 6.4. Whole seedling rotates during data capture.

(e) Thin roots - These are seen in a few cases and tend to be half or quarter the thickness of healthy regular roots and are generally rejected as bad data (figure 6.3).

(f) Random growth of roots - There are cases where the root or the hypocotyl curl around, which makes any curvature or angle measurements a challenge and so these seedlings are rejected as outliers.

(g) Seedling shifting / rotation - The seedlings, due to the force generated by the turning of the root tip and the hypocotyl simultaneously cause the seedlings to

rotate (see Fig 6.4), this may cause erroneous angle measurements. In addition, the germinating seedling may shift from the original planted location of the seed. In most cases the system can still identify the root and root tip.

(h) Condensation Effects - During an experiment condensation builds up on the inside of the Petri dish lid (on the face devoid of the agar growing medium). This condensation build up negatively affects the image intensity and contrast and therefore the performance of many automated thresholding techniques.

The "error conditions" listed above impact overall performance and some situations may be improved by revising our experimental planting procedures. The movement of the seeds, as discussed in 6.3.1(g) can shift them from their original planted location by 2 to $4mm$. Thus making servoing a necessity to locate the seedling, root and root tip. Another, challenge that needed to be resolved was the large vibrations that are generated when moving that large gantry at high speeds. This problem has been resolved by providing ample settling time during data gathering (shown in equation (6.5)).

6.3.2. Data Losses due to internal factors (system errors)

In evaluating the *robot* system performance, we exclude the above cases, and assess only the drop in effective yield due to drawbacks in the system. The following situations arise from errors in the robot focus/servo techniques and hence are potential avenues for improved yield.

(i) Out of focus roots - The errors in focusing are primarily due to the fact that the Petri dish and growing media are all transparent. During the focus searching process the focus measure (measuring image contrast) can be affected by

Figure 6.5. Motion blur induced when operating robot at high speeds.

scratches, dust, bubbles in growing media and condensation, all effect the image contrast.

(j) Vibration blur - Blur is seen when the robot speeds are set very high as the jerk generated is large during starting and stopping (shown in Fig 6.5), making it necessary to have a settling time. Currently to avoid having very large settling times the gantry robot is operated at about 30% of the maximum speed.

(k) Blank images - These images result from (1) non germination of the seed causing the servoing to stray (as it cannot find the root tip) and (2) Erroneous identification of a seedling.

6.3.3. Yield analysis

Having derived an equation for the upper limit on the number of seedlings that can be imaged during a given session, the user will be interested in overall yield in the data gathered. This is described as the percentage of seedlings on the cassette that provided image data from which measurements are reliably extracted and used. The effective yield takes into consideration that some seeds in the cassette may not have

germinated or other external non system related issues. The effective yields for three sample gathering sessions are reported in table 6.4.

The effective yield is determined as the percentage of seedlings with useful data collected versus the available "good" (discounting those seedlings that fall into categories (a) to (h)) seedling in the cassette. This metric, only considers the mistakes performed by the system (categories (i) to (l)). From the data collection sessions so far the effective yield has varied from 75% to about 87%. With further improvements to the servoing system the effective yield can potentially be increased by a maximum of 10%.

The effective yield is determined as the percentage of seedlings (with useful data collected) versus the available "good" (discounting those seedlings that fall into categories (a) to (h)) seedling in the cassette. This measure, only considers the mistakes performed by the system (categories (i) to (k)). As the effective yield is an adjusted measure (discounting the non system loss in data collection) it is possible to achieve 100% under ideal system performance. From the data collection sessions so far the effective yield has varied from 75% to about 85%. With further improvements to the servoing and focusing system the effective yield can potentially be increased by about 5%.

The performance of the system as shown table 6.4 is measured in terms of the useful data obtained from a data collection session by the effective yield metric. This is simply the performance adjusted, taking into account that some seedling locations had anomalies that were outside the design scope of the system. Some of these situations are listed below and sample cases are shown in figures.

The effective yield of a data gathering session is measured in terms of the useful data obtained from a data collection session. This is simply the performance adjusted,

Table 6.4. Robotic System Performance

Test #	1	2	3
Seedlings planted	144	144	72
Bad Data/ servo or focus error	18	26	5
Bad Data/ scratch on agar, improper germination, growth outside depth of field	9	11	6
Good data potentially available	135	133	66
Effective Yield	86%	80.5%	92.4%

taking into account that some seedling locations had seedling deemed not "useful" or not "good". Data from a seedling is deemed "useful" or "good" if the root & root tip can be identified and measurements can be reliably extracted. Thus providing information about the number of "good" seedlings for which data was not acquired. Table 6.4 lists three examples of a typical data gathering session and identifies the number of seedlings that were identified as "good" and number of seedlings the system failed to acquire. The seedling data that was not acquired fall into two categories, (a) Data unavailable due to external factors (not related to the robotic system) and (b) Data unavailable due to systemic failures (related to limitation of the hardware or software). These are itemized above in sections 6.3.1 and 6.3.2.

6.4. Throughput Analysis

In order to demonstrate the throughput advantage that the system has over other methods of data acquisition. Another test was performed where 1700 seedling were imaged. The time required was 28 days with one data gathering session per day, accounting for a yield of about 82% . If the same task were performed with a bank of 10 static cameras (as shown in Fig 6.6), with one camera observing one seedling in one Petri dish as used in [19] it would have taken 180 days with one gathering session per day, assuming 100% yield (although this is not realistic, no studies have been reported with actual yield values for static camera systems). Further optimization of the robotic system can lead to an order of magnitude advantage with respect to data gathering time. The number of sessions required for the stationary camera system would vary

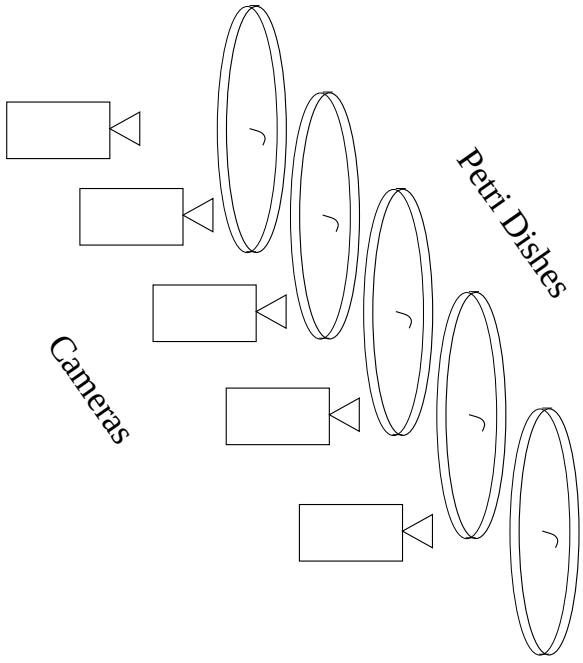

Figure 6.6. Stationary Camera array

with the number of stationary camera units. But the with increase in number of camera units, cost (as can be seen from table 6.1) and logistic issues arise. Additionally,

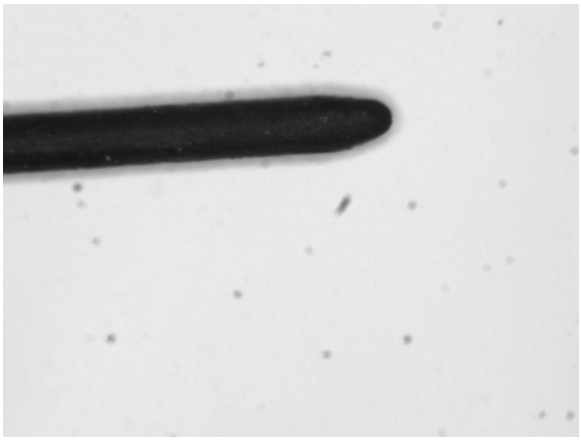

Figure 6.7. Sample image of the artificial root.

the throughput of the robotic system can be further increased (potentially doubled) by planting more than one seedling close to each other such that they are within the field of view of the high magnification camera. There are complications that will arise and further work is currently required to make this scenario work well.

6.5. Evaluation of Feature Extraction

Having documented the design and performance of the system it is also necessary to analyze the variation that can occur in a measured features. The following discussion will show the possible variation in the measured feature values when extracting measurements from images. We start by documenting the the effect of focus on the process of feature extraction both on the intermediate and the final value of the feature interest. As image focus is key to system throughput it is essential to document its effects on the features being measured. We document the effects on the tip angle feature. The analysis will be similar for any other feature that can be extracted. We use a test dataset for the graphs shown in this section. The data set consists of images of an artificial root (which we shall refer to as the "sample"), shown in figure 6.7 that

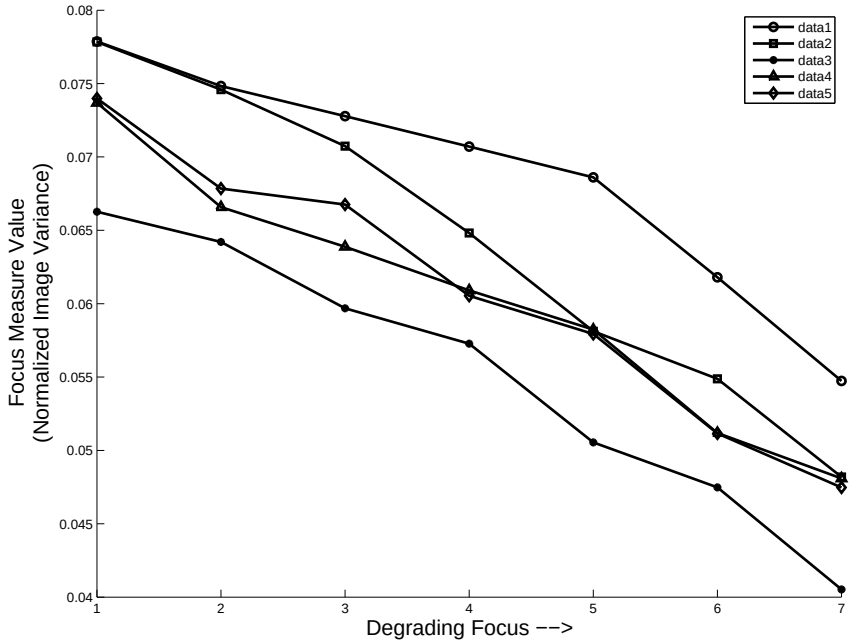

Figure 6.8. The plot shows the change in the computed focus measure. The first value is the image in focus (hence the highest score). The values have not been normalized.

was tubular and straight. The length of the sample was 5 mm and the width was 0.3 mm. The profile of the tip was made to resemble the profile of an arabidopsis root. The camera resolution was adjusted so that the size of the sample in the image was similar to that of an arabidopsis seedling root. The width of the sample in the image was about 60 pixels. The sample was chosen in place of a real root to maintain consistency of ground truth measurements for all the analyses. The images were obtained in a controlled manner. The sample was mounted on a rotary stage that was capable of rotations at a resolution of 0.5 degrees. The rotary stage was adjusted to position the sample horizontally (with respect to the image axes). The angle at this position was used as the zero or reference angle, a_0. The rotary stage was adjusted to different position $\tilde{a}_1$, $\tilde{a}_2$, ... corresponding to 1, 2, 3, 5, 6, 8, 10, 13, ... degrees. Where $\tilde{a}_i$ is $a_i - a_0$, the adjusted or change in angle from the reference orientation, a_0. At each

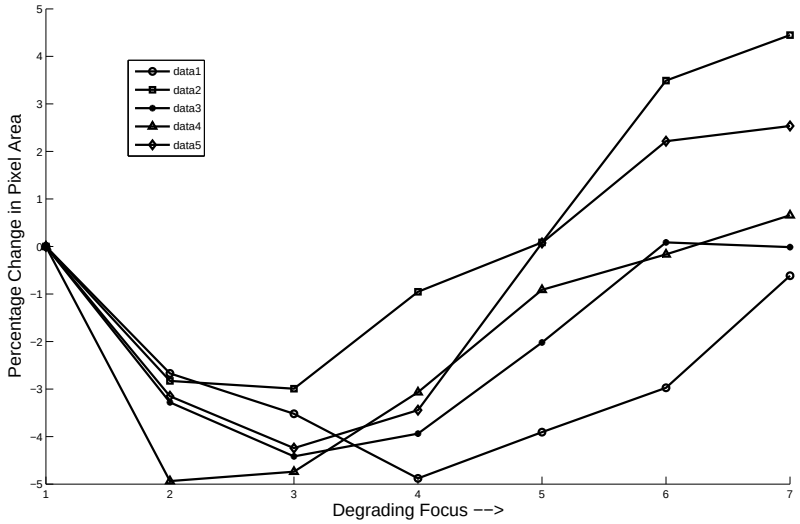

Figure 6.9. Change in area of binarized image due to change in focus. The plot shows change in area of the binarized root (with respect to the area of the root when in sharp focus, i.e. data at focus point 1) as the focus is changed from sharp (in focus) to out of focus (data at focus point 7).

orientation $\tilde{a}_i$ the focus was varied by adjusting the distance between the camera and the sample and thus 7 different focus position were obtained. Figure 6.8 shows the variation in the normalized variance focus measure (as per equation (4.2.3)) computed for the images. The plots are organized to show the effect of quality of the images on the different image processing techniques used at different stages of analysis and on the final feature of interest (the root tip angle).

6.5.1. Effect of Changing Focus on Binarization

The change in the focus can effect the output of the all the image processing steps from binarization to the extraction of the tip angles. Figure 6.9 shows the change in the area of the binarized image occupied by the root with change in the focus. The different curves correspond to roots at different orientations. The values plotted

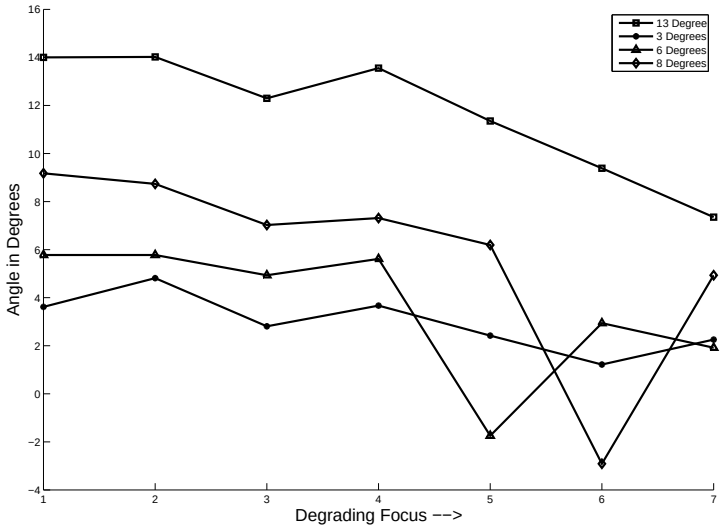

Figure 6.10. Changes in tip angle calculated using a spline fitted to the skeletonized root as focus varies from crisp to blurred.

are the percent change in the area (as compared to the image that is in focus). The ordinate is numbered 1 to 7 to indicate that the images are in descending order of focus quality (as plotted in figure 6.8. Image 1 is in focus and in image 7 the root is almost blended into the background. Curves in figure 6.8 show that the change in focus measure value is about 50 to 60% but the binarized images using the techniques described in the section 4.2.1 show a variation of about 5 to 7%, making the technique very stable and robust in the presence of focus blurring.

6.5.2. Effect of Focus on measured tip angle

The tip angle is extracted from the binarized image using the series of steps described in section 5.1. The quality of the acquired image has an impact on the the binarization which causes variations in the computed tip angle. Figure 6.10 shows the tip angle variation as extracted from one stack of five sample orientations of a test

root-like object obtained at seven different focus qualities. The images are numbered 1 to 7 in decreasing focus quality (depicted on the ordinate of the figures). The angle variations are shown in degrees with respect to the first orientation of the test root. From the plot image 1 (on the ordinate) is the image that is in focus and the angles computed from them are close to the expected values (although 1 to 3 degree changes can still be difficult to extract unless image quality is close to ideal). The difference is due to the imperfections in positioning, rotation and lighting. As the focus degrades the values shift. When the focus is most poor the variation in computed value is about 4 to 5 degrees (the variation includes the variation due to the binarization). Thus small changes in the orientation (1, 3 and 5 degrees) cannot be reliably extracted. Orientation changes on the order of 10 degrees can still be computed from poorly focused images.

If we use out-of-focus images for data gathering and only measure changes on the order of 10 degrees, we can save a precious few seconds on each seedling during the first pass and save time spent on focusing. This would allow for the an increase in throughput from $N = 80$ to $N = 120$ (using equation 6.7).

The smallest changes in angle values that can be reliably extracted (unless ideal conditions are available) are about 5 degrees. For a typical seedling a change in tip angle value by about 5 degrees takes about 18 min. Currently, the system takes about 17 min for the first pass. This would imply that the system, although takes only one image per seedling on the grid for the first 17 min, will be able to measure the changes occurring to the root tip angle during that time. Thus any further improvements to the timing of the first pass will not drastically improve the accuracy of the tip angle curves.

6.5.3. Effect Image Resolution on Computed Tip Angles

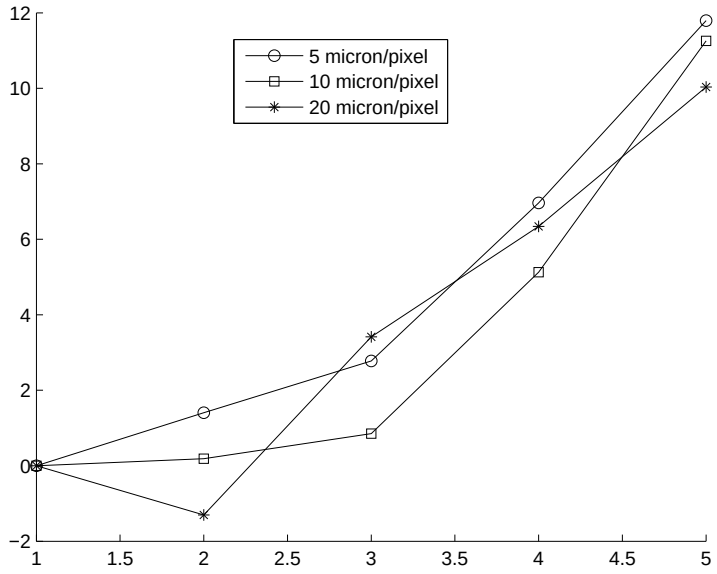

Figure 6.11. Changes in tip angle due to change in Image Resolution.

In addition to focus we also test the effect of image resolution on the measured feature. The image resolution here refers to the number pixels in the image and it does not directly indicate the quality of the image. The image quality is governed by the CCD sensor of the camera and the quality of the lens system used. In figure 6.11 the curves show the same stack with tip angle values extracted with different images at three different resolutions. The values have been plotted with reference to the first image (at time point 1). The average deviation is about 1.2 degrees and the maximum error can be seen to be about 3 degrees.

Figure 6.12 shows the variation in computed angle as the level of focus changes. The change in focus does not cause a significant change in the computed values for different image resolutions as compared to the actual value of the orientation. The overall variation seems to be around 2 degrees.

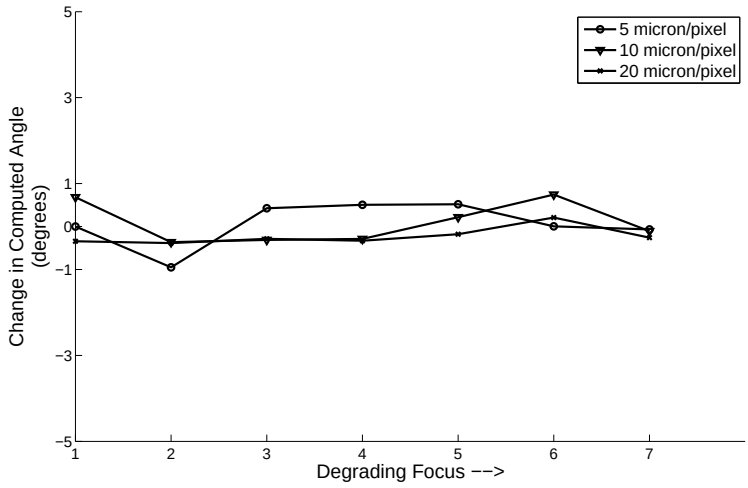

Figure 6.12. Variation in tip angle due to change in Image Resolution, shown at different levels of focus.

6.5.4. Robustness of Root Skeleton and Splines

To demonstrate the robustness of the calculation of root tip angle it is necessary to document the robustness with which the root tip can be estimated. The root tip is determined by the end point of the root's skeleton. The angle is computed by fitting a b-spline curve to the skeleton and using the angle at the tip of the b-spline (or near the tip of the b-spline curve). Figure 6.13 shows a set of test root images binarized by manually varying the threshold on a single gray scale root image. It can be seen that the size and shape of the root changes significantly. Figure 6.14 shows the b-spline representation of the skeleton of the roots, as computed from each of the binary images shown above in figure 6.13.

The plots in figure 6.14 show that the variation in the computed tip is very small. The overall difference in the pixel position of the root tip between the images was computed to be about 1.2% in the x direction and about 0.4% in the y. This equals to about 15 pixels in the x direction and about 4 pixels in the y direction, in a

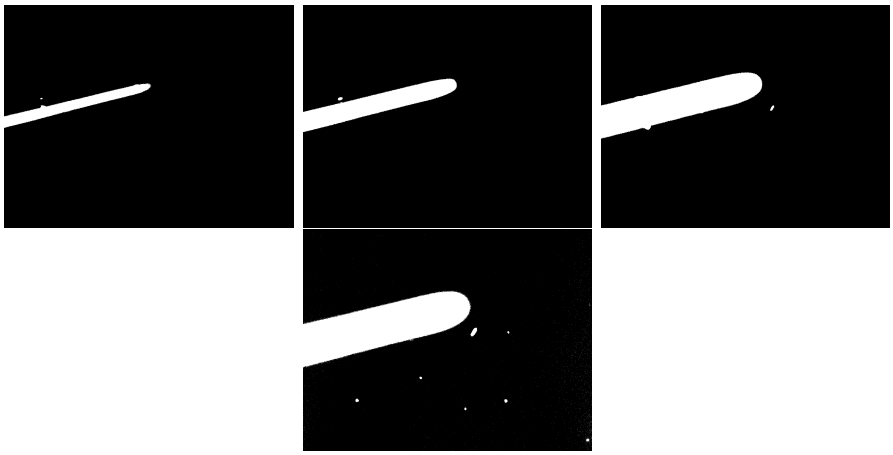

Figure 6.13. Effect of manual choice of threshold on binarization.

1280x960 pixel^2 image. The variation is greater in the x direction because 1) the root is horizontal in the image, 2) the binarization causes a drastic change in the outline of the root. The variation in the outlines are as little as 50 pixels and can be as large as 100 pixels. These variations in the outline cause the skeletal representation to vary. Another reason for the variation is the error in registering skeletal representations when combining them into one plot for comparison.

Figure 6.15 shows the variation in the computed tip angle from these b-spline approximated roots. The images were obtained by turning a rotary stage 10 degrees. The variation in the angle values can be seen to be within a 2.5 degree range.

6.6. Summary of Analysis and Conclusions

6.6.1. Summary of Evaluation

In this chapter we have analyzed the working and the performance of the system. We have shown that the developed system is cost effective to build and setup. The timing analysis showed that depending on the biological process being observed, the

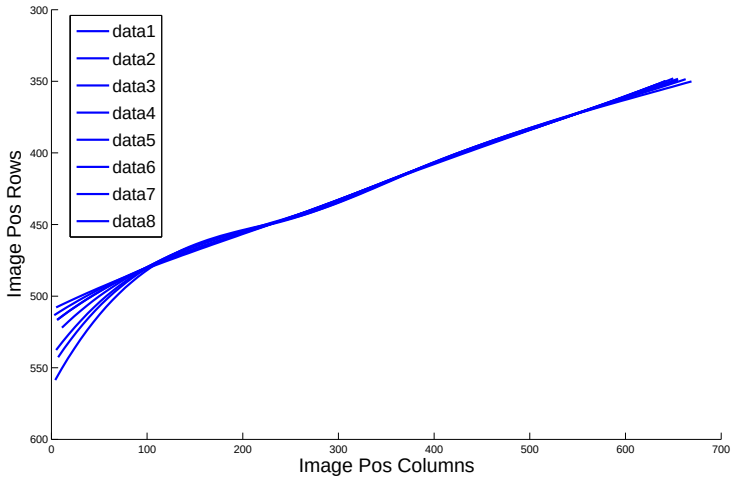

Figure 6.14. Changes in spline and skeletal representation due to changes in manually chosen thresholds for binarization. The overall variation in tip of the skeletal representation of the root is 1.5% in the x axis (20 out of 1280 pixels) and 0.5% in the y axis (4 out of 960 pixels). A portion of the variation is due to errors in registering the skeletal pixels.

maximum number of observable seedlings can be determined. We have documented the losses that occur during data gathering and have shown that the effective yield of the system is higher than what would have been possible with the static camera setup currently used. We have subsequently identified the system's bottlenecks and improved the design to reduce the effect of the bottleneck and have suggested other avenues for improvement.

The analysis has also evaluated the effect of focus blur, image resolution and time resolution with respect to a feature of interest, the feature considered here is the root tip angle. From the discussion of the trends observed in the plots it can be inferred that for good quality (or in-focus) images the variation in computed values is about 2 degrees. If the images are blurred (to about 60% of the max focus quality) the variation can be at most 5 to 6 degrees.

The measured root tip angles are robust only when the changes in the root tip angle are more than the variation in the measurement technique. This variation, as

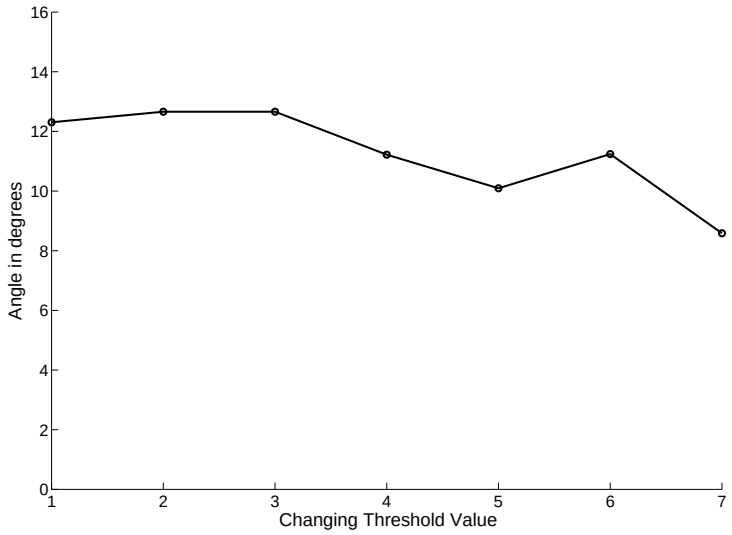

Figure 6.15. Changes in computed tip angle when using a spline and skeletal representation with changes in manually chosen thresholds for binarization. The true orientation of the root is 10 degrees. Some amount of the error can be attributed to positioning inaccuracies with the rotary stage where the step size is 1 degree.

documented above, is about 5 to 6 degrees. The approximate time taken by the root tip to turn 6 degrees is about 10 to 15 minutes. To ensure that changes on the root tip are sufficiently captured at least one image of the root must be obtained every 14 minutes.

The robustness of the skeletonization and the spline fitting with respect to location of the tip, stability in the presence of blur and image resolution has been described. The variation was found to be within 2%. The discussion shown above are critical as they allow us to evaluate the system and compare data extracted using this system with data that may be extracted by any other technique. In addition all the analysis described above can be followed to calibrate measurements made with any other image analysis techniques.

6.6.2. Discussion of System Design Choices

The system in its current state provides an increase in throughput by about one order of magnitude. The number of seedlings that can be imaged, ranges between 72 and 144 (2 or 4 seedlings per dish). It may be possible to plant more seedlings per Petri dish, which would reduce the number of Petri dishes required to plant the seedlings thus reducing the workspace required for the robotic system. This would be possible only in the case of seedlings that are of size similar to the arabidopsis seedlings. For seedlings larger than arabidopsis fewer seedlings per Petri plate would result in larger work space requirements.

As discussed in earlier sections the process of focusing, using a lens system with very small depth of field (1-2mm), to obtain sharp images is one of the primary bottlenecks of the system. During the initial development and testing stages numerous techniques were tested in order to reduce the effect of the bottleneck. The following is a list of techniques explored to tackle focusing problem.

1. Placement of spherical beads (of known dimension) in the agar medium in order to aid in focusing and depth estimation.

2. Place a calibrated pattern on the surface of the Petri dish to aid in depth estimation.

3. Using a laser depth measurement sensor at the end effector along with the cameras.

4. Manual marking on the surface of the agar to provide and estimate of the region of interest and the surface of the Petri .

Techniques 1 and 2 suffered from a common problem: it was easy to focus on the

beads in the agar or the pattern on the surface of the plate but another focusing step was required to focus onto the root as the distance from the surface of the plate or the beads to the surface of the agar was not a constant and varied from one region of the plate to another. An estimate of this distance can be obtained by obtaining ground truth measurements from a large number of Petri plates, however using this estimate to move the camera still required a confirmation test to determine if the root was in focus or not. Technique 3, using the laser to measure depth proved to be of little help. The depth measurements proved to be very erratic as the plastic, agar growth media and all the parts of the PDCU were transparent making the depth measurements unreliable. Technique 4 was a plausible solution when using only a small number of Petri dishes. Marking 36 dishes with 2 to 4 seedlings per dish, involved a large amount of manual labor. In addition, a lot of care was need to avoid disturbing or dislodging the seedlings, as the markers had to be placed in a region 1 or 2 mm away from the seedling. All of these techniques either made the focusing process more complicated or added a significant amount of manual labor. Hence a purely image based approach was adopted to perform the focusing process. Initial attempts at determining sharp focus were directed towards the detection of high frequency content in the images. A fast Fourier transform (FFT) of the image was used to determine its frequency content and judge the extent of focus. This was a slow computational process and was not suitable for repeated computation. Also the peak value used to determine the sharp focus was biased towards the presence of root hairs. The focus measure derived from FFT computation was more suited to determine if the root hairs were in sharp focus or to determine if the noise content in the image was very high. A simple variance measure (as discussed in section 4.2.3) was adopted. The next step in focusing was to determine a technique to vary the extent of focus. Two focusing techniques were

tested

(a) Adjusting the focal length of the lens.

(b) Moving the camera to adjust the location of the focal plane.

Although, technique (a) was the fastest of the two methods , it proved to be difficult to use. This was due to the drifting of the seedling out of the field of view when adjusting the lens for focus. The drift occurs when adjusting the lens elements, which may not be perfectly optically aligned. In many cases a simple servoing task would correct the drift. But in some cases the seedling would move out side the field of view and a search would have to be performed to determine its location, voiding the speed up gained in focusing. Also, a calibration step would be required once focal length was adjusted, before any metric information can be obtained from the captured image. Hence technique (b) was chosen for its simplicity.

From the graphs and their discussions in section 6.5 presented above it can be inferred that by relaxing the requirement on sharpness of focus we can increase throughput by reducing the time spent searching for the best focused image. By relaxing the image resolution, in terms of magnification, requirement the field of view and depth of field can be increased. This will allow more than one seedling to be (present in the field of view) imaged at a given location and reducing the time required to bring a seedling into the depth of field of the lens. These two adjustments to the requirements will have a multiplicative effect on the overall throughput of the system.

6.6.3. Seedling and the Automated System

Considering that the entire systems has been designed, built, tested and analyzed with respect to the seedling it is required to relate all the information obtained from

the above analysis (in this chapter) to the type of seedling being considered. The *Arabidopsis Thaliana* seedlings, 3 to 4 days after germination are approximately 3 to 5 mm long and vary from 50 microns to 200 micron in thickness. From the analysis presented in section 6.5 we can infer that the accuracy of the feature extraction is sensitive to focus only when the image blur is significantly close to 70% of the peak value. The other factor that neeeds to be considered when the accuracy in computed values is of concern is resolution which is determined by the magnification of the lens. The current resolution of the camera is about 5 microns per pixels. From figure 6.11 we can see that even if the resolution is changed by a factor of four to 20 microns per pixel the change in computed tip angle value is about 3 degrees. Thus, as long as the optics is adjust so that the image of the root of the seedling is at least 5 to 12 pixels wide in a given image, the error in computed tip angle will be about 3 degrees or less. For seedlings with root width ranging from 50 to 200 microns the camera resolution will have to be about 10 microns per pixel (between the high and low values). Having images with higher resolution will not necessarily produce significantly better results (lower error).

Chapter 7

Future Work

Chapters 1, 3 and 4 have discussed in detail the design and the construction of the system. Chapter 2 described the components of the high throughput pipeline and a case study of a typical data gathering session. Analysis of the system was discussed in chapter 6. This system, as described in the preceding chapters has been designed to conform closely to the ideal specification for the extreme scenario presented due to the combination of the following requirements when working with seedlings of *Arabidopsis thaliana* (seedlings of small size).

- Ability of the robotic system to support micron level positioning accuracy at high speeds (up to 1 m/s), with payloads of up to 10 kgs, for large work spaces (1m $\times$ 1m).
- Small size of seedlings (5 mm long and 50 to 200 microns wide).
- Camera lenses with small depth of field (1 mm approx.).
- With high spatial and temporal resolution of data capture.
- Adaptability to seedlings of various sizes.

- Adaptability to monitor other phenotypes in seedlings.

Based on the detailed description of the system and analysis of its capabilities and shortcomings presented in the preceding chapters here we discuss avenues for possible extensions and future directions for research.

- Relax focus and camera resolution requirements - The maximum impact and immediate gain for the system would be in testing the maximum throughput that can be gained by relaxing the focus requirement and reducing the resolution of the camera as discussed at the end of section 6.6.2. With the easing of the focus requirement the time taken to focus during the first pass can be reduced (a 2 second reduction per seedling can reduce the first pass time by up to 2.5 minutes). The throughput can be further increased if the image resolution can be decreased (analysis showed that a reduction by a factor of 2 produced 1 to 2 degree changes in computed tip angle values). The reduced resolution will increase the field of view allowing 2 or more seedlings to be imaged simultaneously, effectively doubling the throughput.

- Feature Extraction - One key area for extensions for the system is to add the required image processing techniques for extracting other features from root images, e.g. curvature of the root, growth rate, onset of root hair growth and their count, etc. These are features that can be readily extracted from the images that have already been gathered. Thus providing an extended and rich feature set to analyze for phenotypes. Such techniques could be incorporated with ease into the workflow with very little modifications, improving the capability of the system. However, the sensitivity of each additional feature would need to be tested to determine the effects of system parameters on its computed values

similar to the analysis performed for the tip angle measurements performed in section 6.5.

- Altering design specifications to suit the seedling - Altering the specifications of the robotics hardware to suit the specific task of seedling root phenotyping (or any specific phenotype) rather than having a single versatile system capable of analyzing many phenotypes needs to be considered. This will allow the system to be specially designed to generate high quality, high throughput data of a very specific feature, e.g. a robotic system to only collect root features for arabidopsis seedlings, a separate system to collect root features from other plant species etc. This would allow for a system suited for arabidopsis seedlings to be smaller and more compact compared to a robotics system for maize, e.g. the workspace requirements for a system catering to only arabidopsis root features could have a smaller workspace, thus a smaller sized robot. If we use the 72 seedlings (as used in this thesis) with 8 seedlings planted per Petri dish, only 9 dishes would be required which would translate to a workspace half the size of the current system. However, the throughput, the time analysis and all other aspects of the system would remain the same. Smaller work space may impact cost of construction and laboratory space requirements. The difference would be in the versatility, e.g. the current system can be adapted to collect data from seedlings of various size.

- Add environmental control capabilities - The capabilities of the system can be extended by modifying the design of the PDCU to allow control of environmental conditions (e.g. temperature, humidity and lighting, circadian cycles) in each compartment of the PDCU by adding sensors to monitor and control

the environment around the Petri dish. These modifications will allow the plant biologist to study the effects of even small changes in environmental conditions on the phenotypic features of interest.

- Use GPU computing power - The post processing parts of the workflow namely, feature extraction and phenotype analysis consume a considerable amount of time. If the image processing techniques were modified to run on a GPU, processing times can be significantly reduced. If the processing can be optimized to run during the data gathering stage, image quality can be determined online. This may allow the data gathering system to capture an image, check the quality and adjust for focus or position to obtain images that produce smaller errors in the computed features.

- Database to optimize workflow - The automated system collects large quantities of image data (each run generates about 13 gigabytes of image data) and corresponding meta data, from experimental information to extracted feature information. A well designed relational database system (RDBMS) would be invaluable in storing and accessing the information while maintaining data consistency and reducing errors that can occur due to manual data handling. The RDBMS could be used to track the performance of the pipeline and be designed to optimize the workflow. The RDBMS could be designed to replace the scheduling portion of the current workflow. This would need careful and rigorous testing because it has the potential to generate large quantities of junk database entries making the task of database management very tedious.

- Multiscale Data Gathering - The phenotyping system is currently used to gather phenotypic data from the root of seedlings at one resolution, but it has been

designed to obtain images of the root and entire seedling simultaneously (which is currently not used). This multiscale data acquisition can be used for correlation studies, to correlate root phenotypes to hypocotyl phenotypes, or phenotypes from root systems (having multiple secondary roots which are present in seedlings older than 4 to 5 days). These studies are hard to perform with other systems as multiple images with varying resolution will have to be recorded concurrently. The robotic system is ideal for such scenarios. A viable extension to the current system would be to mount a microscope to the end effector of the robot in addition to the 2 cameras. The microscope could be used to obtain images with cell level resolution concurrent to the root and seedling data. These data sets would allow more detailed correlation studies (from the entire seedling to specific portions of the seedling, down to the activity in particular groups of cells in a region of the seedling). The addition of the microscope may introduce some complications in focusing and may effect the throughput. The techniques developed in the present system could be used for the microscope system but will need carefully testing.

- Data gathering in 3D - The robotic system has been designed to carry a large payload. This allows for the additional cameras to be attached to the end effector. The additional cameras can be used to capture data in 3D with no added impact to the throughput of the system. The 3D data can be used to obtain more features or phenotypes from the shape of the roots (e.g. twist in the root as it turns in response to a gravitropic stimulus), hypocotyls, or 3D shape of the cotyledons of the seedlings. The 3D images can be gathered at multiple scales as well (as described above). The system in its current state can acquire small baseline stereo images (by translating the camera by a fixed distance) with

almost no modification. These can be used to generate 3D data. However, the necessary software for stereo reconstruction will have to be developed and tested.

- Phenotyping various seeds/seedlings - The system described in this thesis has been designed to be versatile and modular. The system it can be adapted with little or no modifications to either the hardware or software to be used with seedlings of plant species other than arabidopsis, e.g. maize, rice, tomato, etc. Although the modifications, if required, required would be minimal, they will need to be implemented and rigorously tested prior to being integrated into the workflow. The design changes could range from small modifications to the segmentation algorithm to redesign of the PDCU to accommodate the size of the seedling.

- Automate Petri Dish Preparation - With increase in throughput capabilities it is possible to gather data from 100 seedlings concurrently. This increase in throughput demands a consistent supply of seedlings grown in Petri dishes to be made available, to maintain constant high throughput data acquisition. A large number of Petri dishes must be prepared on a regular basis. With the current system, when performing one 8 hour data collection system per day with 36 Petri dishes per session (2 seedlings per dish) a total of 108 Petri plates will need to be handled every day (depending on the experimental condition). If more than one session is carried out per day the numbers double. The task of preparing the Petri dishes with growth medium and planting seeds becomes a very daunting task. The pouring of media into Petri dishes and planting of seeds is a repetitive task well suited for a robotic system. Such a system might prove necessary when data gathering throughput increases further.

BIBLIOGRAPHY

[1] N. Andreff, B. Espiau, and R. Horaud. Visual servoing from lines. In *In International Conference on Robotics and Automation, San Francisco*, April 2000.

[2] P. Basu, J. Pal, J.P. Lynch, and K.M. Brown. A novel image-analysis technique for kinematic study of growth and curvature. *Plant Physiology*, 145:305–316, October 2007.

[3] J. F. Canny. A computational approach to edge detection. *IEEE Trans. Pattern Analysis and Machine Intelligence*, 8 (6):679–698, 1986.

[4] F. Chaumette. Image moment: A general and useful set of features for visual servoing. *IEEE Transactions on Robotics*, 20(4):713–723, August 2004.

[5] F. Chaumette and S. Hutchinson. Visual servo control, part i: Basic approaches. *IEEE Robotics and Automation Magazine*, 13(4):82–90, December 2006.

[6] F. Chaumette and S. Hutchinson. Visual servo control, part ii: Advanced approaches. *IEEE Robotics and Automation Magazine*, 14(1):109–118, March 2007.

[7] A. Chavarria-Krauser, K.A. Nagel, K. Palme, U Schurr, A. Walter, and H Scharr. Spatio-temporal quantification of differential growth processes in root growth zones based on a novel combination of image sequence processing and refined concepts describing curvature. *New Phytologist*, 177:811–821, 2008.

[8] A. French, S. Ubeda-Tomas, T. Holman, M. Bennett, and T. Pridmore. High-throughput quantification of root growth using a novel image-analysis tool. *Plant Physiology*, 150:1784–1795, August 2009.

[9] F. Groen, I. Young, and G. Ligthart. A comparison of different focus functions for use in autofocus algorithms. *Cytometry*, pages 623–691, 1985.

[10] M. Hall, E. Frank, G. Holmes, B. Pfahringer, P. Reutemann, and I. Witten. The weka data mining software: An update. *SIGKDD Explorations*, 11 (1), 2009.

[11] S. A. Hutchinson, G. D. Hager, and P. I. Corke. A tutorial on visual servo control. *IEEE Trans. Robotics and Automation*, 12(5):651–670, Oct 1996.

[12] H. Ishikawa and M. Evans. Novel software for analysis of gravitropism: Comparitive response patters of arabidopsis wide-type and axr1 seedlings. *Plant Cell Environ*, 20:919–928, 1997.

[13] M. Jaffe, A. Wakwfield, F. Telewski, E. Gulley, and R. Biro. Computer-assisted image analysis of plant growth, thigmomorphogenesis and gravitropism. *Plant Physiology*, 77:722–730, 1985.

[14] M. Kristan, J. Pers, M. Perse, and S. Kovacic. A bayes spectral entropy based measure of camera focus using a discrete cosine transform. *Pattern Recognition Letters*, 27:1431–1439, May 2006.

[15] E. Krotkov. Focusing. *IJCV*, 1:223–237, 1987.

[16] L. Lam, S. Lee, and C. Suen. Thinning methodologies - a comprehensive survey. *IEEE Trans. Pattern Anal. Mach. Intell.*, 14(9):869–885, 1992.

[17] LemnaTec. http://www.lemnatec.com, 1998.

[18] R. Mahony, P. Corke, and F. Chaumette. Choice of image features for depth-axis control in image based visual servo control. In *Proceedings of the IEEE Conference on Intelligent Robots and Systems*, pages 390–395, October 2002.

[19] N. Miller, B. Parks, and E. Spalding. Computer-vision analysis of seedling responses to light and gravity. *The Plant Journal*, 52(2):374–381, October 2007.

[20] T. Mitchell. *Machine Learning*. McGraw Hill, 1997.

[21] G.B. Monshausen and S. Gilroy. Feeling green: mechanosensing in plants. *Trends in Cell Biology*, 19:228–235, 2009.

[22] R. Moore, D. Clark, and D. Vodopich. *Botany*. WCB/McGraw-Hill, 1998.

[23] J Mullen, C Wolverton, H Ishikawa, and M Evans. Kinetics of constant gravitropic stimulus responses in arabidopsis roots using a feedback system. *Plant Physiology*, 123:665–670, June 2000.

[24] N. Nathaniel, P. Neow, and H. Ang Jr. Practical issues in pixel-based autofocusing for machine vision. In *ICRA*, page 2791, 2001.

[25] N. Otsu. A threshold selection method from gray-level histograms. *IEEE Trans. Sys., Man., Cyber*, 9:6266, 1979.

[26] D. Schmundt, M. Sitt, B. Jahne, and U. Schurr. Quantitative analysis of the local rates of growth of dicot leaves at a high temporal and spatial resolution, using image sequence analysis. *Journal of Plant Growth Regulation*, 16:505–514, 1998.

[27] J. Shi and C. Tomasi. Good features to track. In *Proceedings of the IEEE Conference on Computer Vision and Pattern Recognition*, pages 593–600, 1994.

[28] Y Song and L. Sun. A new auto focusing algorithm for optical microscopebased automated system. In *ICARCV*, 2006.

[29] Y Sun, S Duthaler, and B. Nelson. Autofocusing algorithm selection in computer microscopy. In *Proceedings of the IEEE Conference on IROS*, 2005.

[30] O. Tahri and F. Chaumette. Point-based and region-based image moments for visual servoing of planar objects. *IEEE Transactions on Robotics*, 21(6):1116–1127, December 2005.

[31] C. vn der Weele, H.S. Jiang, K.K. Palaniappan, V.B. Ivanov, K. Palaniappan, and T.I. Baskin. A new algorithm for computational image analysis of deformable motion at high spatial and temporal resolution applied to root growth. roughly uniform elongation in the meristem and also, after an abrupt acceleration, in the elongation zone. *Plant Physiology*, 132:1138–1148, July 2003.

[32] A. Walter, H. Spies, S. Terjung, R. Kusters, N. Kirchgebner, and U. Schurr. Spatio-temporal dynamics of expansion growth in roots: automatic quantification of diurnal course and temparature response by digital image sequence processing. *Journal of Experimental Biology*, 53:689–698, 2002.

[33] L. Wang, I.V. Uilecan, A.H. Assadi, C.A. Kozmik, and E.P. Spalding. Hypotrace image analysis software for measuring hypocotyl growth and shape demonstrated on arabidopsis seedlings undergoing photomorphogenesis. *Plant Physiology*, 149:1632–1637, 2009.

[34] C. Wolverton, H. Ishikawa, and M.L. Evans. The kinetics of root gravitropism: Dual motors and sensors. *Journal of Plant Growth Regulation*, 21:102–112, 2002.

[35] P.T. Yap and P. Raveendran. Image focus measure based on chebyshev moments. *IEE Proc.-Vis. Image Signal Process.*, 151(2):128, April 2004.

[36] T. Y. Zhang and C. Y. Suen. A fast parallel algorithm for thinning digital patterns. *Communications of the ACM*, 27 (3):236–239, March 1984.

APPENDIX A

MATERIALS SOURCE AND SPECIFICATIONS

Item	Company
PDCU Polycarbonate Sheets	**Larid Plastics** *http://www.lairdplastics.com*
PDCU Machining	**Trace-A-Matic Corporation** *http://www.traceamatic.com*
LED Grow Lights and Fittings	**Super Bright LEDs Inc.** *http://www.superbrightleds.com*
PDCU Frame	**80/20 Inc.** *http://8020.net*

Table A.1. PDCU Parts Source List. Web links accessed May 2012.

Item	Company
Linear Slides, Support Structure Construction and Misc. Cables	**IntelLiDrives, Inc.** *http://intellidrives.com*
Gantry Master Controller	**Galil Motion Control** *http://www.galilmc.com* (DMC4040)
Controller Software Interface Library	**Galil Motion Control** *http://www.galilmc.com/support/overview.php*
Servo Drive Units	**Copley Controls** *http://www.copleycontrols.com/Motion/index.html* *http://www.copleycontrols.com/Motion/Downloads/xenusData.html* (Xenus XLT-230-18)

Table A.2. Gantry Parts Source List. Web links accessed May 2012.

Parameter	Unit	Z axis	X axis	Y axis
Motor Type		LSM-P-32 -540-50-T	LSM-P-24 -206-50-S	LSM-P-24 -206-50-S
Drive Type (Copley Controls)		XSL-230-36	XSL-230-36	XSL-230-18
Actuator type		LSS-200	LSS-160	LSS-160
Stroke length	mm	1124	1100	200
Peak force (F_p)	N	1735	645	645
Continuous force	N	766	225	225
Peak Current	A_{rms}	16.7	14	14
Continuous Current	A_{rms}	6.8	4.7	4.7
Max speed @ F_p	m/s	1	1.5	1.5
Max Acceleration	m/s^2	4	4	2
Brakes (electro magnetic)		2	0	0
Shock Absorbers		2	0	0

Table A.3. Specifications for each axis of the gantry system